

Rimu.jl: Random integrators for many-body quantum systems

Matija Čufar¹ , C J Bradly^{1,2} , Ray Yang^{1,3} , Elke Pahl⁴  and Joachim Brand^{1*} 

1 Dodd-Walls Centre for Photonic and Quantum Technologies, New Zealand Institute for Advanced Study, Massey University, Private Bag 902104, North Shore, Auckland 0745, New Zealand

2 School of Mathematics and Statistics, University of Melbourne, Parkville, Victoria 3010, Australia

3 Department of Chemistry, Washington University in St. Louis, St. Louis, MO 63130, USA

4 MacDiarmid Institute for Advanced Materials and Nanotechnology, Department of Physics, University of Auckland, Auckland 1010, New Zealand

* J.Brand@massey.ac.nz

January 28, 2026

Abstract

Rimu.jl is a Julia package for solving many-body quantum problems. The core of the package is a matrix-free implementation of Hamiltonians and other operators and compact representation of Fock states, which together allow for efficient methods suitable for high-performance computing. Rimu.jl includes a Julia implementation of the full configuration interaction quantum Monte Carlo (FCIQMC) algorithm which is a type of projector QMC algorithm for stochastically solving the time-independent Schrödinger equation. It also includes many well-known model Hamiltonians, and an interface for exact diagonalisation based on external eigenvalue solvers. Both the stochastic and exact diagonalisation methods are accessed with a **CommonSolve.jl** interface. We describe the FCIQMC algorithm and how to obtain estimators of observables as well as the key features of the implementation.

Contents

1 Introduction	2
2 Usage example: a preview of attractions to come	4
2.1 Basic computation	4
2.2 Excited states	6
2.3 Observables	7
2.4 Exact diagonalisation	8
3 The FCIQMC algorithm	9
3.1 A fixed point iteration	9
3.2 Quantum Monte Carlo	10
4 Computing observables	13
4.1 Time-series analysis	13

4.2	Energy estimators	14
4.3	General observables	17
4.4	Reweighting	19
5	Exact diagonalisation	19
6	Data structures	20
6.1	Fock state addresses	20
6.2	Hamiltonians and operators	23
6.3	Dict Vectors	25
6.4	Parallel operations on vectors	26
7	Numerical results	28
7.1	Semistochasticity and vector compression styles	28
7.2	Performance benchmarks	31
8	Conclusion and outlook	33
References		34

1 Introduction

Calculating the ground state of a quantum many-body problem is an important problem with applications in many areas of physics and chemistry. As the Hilbert space dimension of such problems grows exponentially with system size, solving them numerically in a deterministic way becomes intractable already at modest system sizes. However, through the use of stochasticity in Monte Carlo methods, both time and memory requirements of solving a quantum many-body problem can be drastically reduced. The family of methods that use stochastic techniques to solve quantum problems is known as quantum Monte Carlo (QMC). A common feature of the widely varying QMC methods is that they all stochastically sample the solutions to the (deterministic) problem in such a way that taking an average of the recorded samples yields a good approximation of the true solution [1, 2]. A particular class of QMC methods is projector Monte Carlo (PMC), which uses a repeated application of a transition operator to an arbitrary initial state to project out all states but the ground state. Then, in the limit of many applications, the method can be seen as a projector. The transition operator is applied stochastically, and depending on the transition operator used, the basis, and the exact details of the stochastic application, several different variants of PMC can be defined [3]. Some notable examples include Green's function Monte Carlo [4, 5], diffusion Monte Carlo [6], auxillary field quantum Monte Carlo [7], path integral ground state [8], and full configuration interaction quantum Monte Carlo [9].

Full configuration interaction quantum Monte Carlo (FCIQMC) [9] was first developed for use in quantum chemistry to solve problems related to the electronic structure of molecules, solid state applications, and Hubbard models. Although the algorithm has mostly been used in these areas [10–13], it has been successfully applied to problems relating to the physics of ultra-cold quantum gases [14–17] and, due to its simplicity could be applied to find the lowest eigenpair of any matrix in general. A major advantage of

FCIQMC over other PMC algorithms is that it can treat problems with a sign problem without resorting to approximations like the fixed-node approximation, assuming a sufficiently large amount of resources is employed. Another big advantage is that FCIQMC it has no time step error, if the time step is small enough, such that no extrapolation to small time steps is needed. Several variants of FCIQMC exist: The original formulation [9], which is no longer in use, used integer coefficients, where each unit of the coefficient was treated as an independent walker. This was later extended to real (floating-point) coefficients with a semistochastic formulation [18] where a part of the Hilbert space is treated exactly with the rest sampled stochastically. Further expansions of the algorithm include the initiator approximation [19, 20], which trades the sign problem for a small bias, importance sampling [21, 22], which reduces the inherent population control bias present in FCIQMC, methods of improving convergence speed [23, 24], heat bath sampling [25], which samples matrix elements with probabilities proportional to their value, and the fast randomised iteration approach [26, 27], which improves the way an FCIQMC vector is compressed. In addition to computing ground state properties, variants of FCIQMC can also be used to compute excited states [28], density matrices [29], or even real-time dynamics [30]. There exist several open-source implementations of FCIQMC focused on electronic structure problems [31–33].

In this paper, we present Rimu.jl, a Julia [34] framework for working with quantum many-body systems with a focus on FCIQMC and exact diagonalisation. We present the variant of the FCIQMC algorithm employed by Rimu.jl, which dynamically determines the size of the deterministic subspace. Further, we describe the data structures used and show results of numerical benchmarks measuring the effects of the various parameters exposed by Rimu.jl, and its performance on thread-parallel and MPI [35]-distributed computer systems is described.

We have designed the package to work with more general quantum many-body Hamiltonians beyond the electronic structure problem. Specifically, our own research interests are motivated by ultra-cold atom systems. To facilitate this, Rimu.jl is defined to work with arbitrary mixtures of (possibly non-number conserving) bosons and fermions with arbitrary spins. However, our package also supports working with spin-1/2 fermions and thus molecular Hamiltonians. Extending the capabilities beyond the currently implemented Fock-state bases is also supported through the implemented type hierarchies and interfaces.

The benefits of implementing in Julia are many, but in our case the most valuable is the multiple dispatch feature, which allows us to tweak the internals of the implemented algorithms without having to modify the main code base. This speeds up development, and makes it easy to experiment with the algorithm and develop prototypes. Multiple dispatch also allows us to use type-level metaprogramming to have the Julia compiler generate specialised code tailored to the simulation parameters. Additionally, the input file for Rimu.jl is simply a Julia script, which makes working with Rimu.jl easy.

This paper is organised as follows: In Sec. 2, we start with an example showing some of the features of Rimu.jl and giving the reader an idea about how Rimu.jl is used. Then, in Sec. 3, we discuss the variant of the FCIQMC algorithm employed by Rimu.jl in detail, starting with a deterministic version, and then introducing stochasticity. In Sec. 4, we discuss the various statistical techniques that allow us to extract useful information from an FCIQMC computation. This includes various ways of estimating the energy of a system or its observables. We briefly present the two major ways exact diagonalisation can be performed with Rimu.jl in Sec. 5. In Sec. 6, we dive into the implementation details of the data structures used for representing Fock states, operators and vectors. We discuss how these implementation details allow for efficient FCIQMC and exact diagonalisation. In Sec. 7, we present numerical results showing how algorithm parameters affect an FCIQMC

calculation, and present benchmarks of the performance of Rimu.jl with thread-parallel and MPI-distributed calculations. Finally, in Sec. 8, we conclude the paper and present possible future directions for Rimu.jl.

2 Usage example: a preview of attractions to come

We begin with a short example of an FCIQMC computation with Rimu.jl, linking to the relevant parts of this paper every time a new concept is introduced. We will use the Bose-Hubbard model, which is a standard model in many-body physics that captures the important properties of the superfluid–Mott insulator transition [36]. As a simple case, consider the one-dimensional Bose-Hubbard Hamiltonian for fixed particle number

$$\hat{H} = -t \sum_{\langle i,j \rangle} \hat{a}_i^\dagger \hat{a}_j + \frac{u}{2} \sum_{i=1}^M \hat{n}_i (\hat{n}_i - 1), \quad (1)$$

where \hat{a}_i^\dagger (\hat{a}_i) creates (destroys) a particle on site i , $\hat{n}_i = \hat{a}_i^\dagger \hat{a}_i$ is the particle number operator, $\langle i,j \rangle$ denotes all pairs of adjacent sites, and t and u are dimensionless hopping and interaction parameters, respectively. In this example, we will look at a system of $N = 12$ particles in $M = 12$ sites, which results in a Hilbert space dimension of 1,352,078. This is small enough to be quickly solvable with Rimu.jl’s FCIQMC and sparse eigenvalue solvers, but too large for dense numerical linear algebra. In the example, we will start with a basic computation, then extend it to show computing excited states and observables. Finally, we will use exact diagonalisation and compare the results obtained with these methods.

2.1 Basic computation

If Rimu.jl is not yet installed, we install through the Julia package manager by typing

```
] add Rimu
```

in the Julia REPL. We can now set up the computation by loading Rimu.jl, then creating a bosonic Fock address and defining the Hamiltonian:

```
using Rimu
N = 12 # number of particles
M = 12 # number of sites
address = near_uniform(BoseFS{N,M})
hamiltonian = HubbardRealSpace(address; u=6.0)
```

The Fock address is created first to define the quantum statistics and the Hilbert space of the problem, as discussed in Sec. 6.1. The bosonic Fock state constructed with `near_uniform` is one where the $N = 12$ particles are uniformly distributed across the $M = 12$ modes, which represent lattice sites of the Hubbard model. We then pass the address and the interaction parameter $u = 6$ to the Hamiltonian constructor, while leaving t at its default value of 1. This corresponds to strong on-site interactions typical of the Mott-insulating regime. Passing the address to the Hamiltonian this way sets the number of particles and lattice sites, as well as providing a starting point for the FCIQMC calculation. This is discussed in more detail in Sec. 6.2.

As the simulation runs we will also collect the data required to compute the projected energy, which is an estimator of the ground state energy, as explained in more detail in Sec. 4.2.

```
reference_vector = PDVec(address => 1.0)
post_step_strategy = ProjectedEnergy(hamiltonian, reference_vector)
```

The projected energy requires a reference vector which we set up as a `PDVec` (see Sec. 6.3) with the value of 1 at the starting address here.

Now, we create the `ProjectorMonteCarloProblem`, which holds the information necessary to start an FCIQMC run and solve it with the `solve` function following the `CommonSolve.jl` [37] interface. We finally store the result to a `DataFrame` [38] and display it.

```
problem_fciqmc_basic = ProjectorMonteCarloProblem(
    hamiltonian,
    last_step=10_000,
    target_walkers=100_000,
    post_step_strategy,
)

result = solve(problem_fciqmc_basic)
df = DataFrame(result)

display(df)
# 10000x11 DataFrame
#   Row | step   len   shift      norm      exact_steps  inexact_st ...
#   Int64 | Int64  Float64  Float64  Int64        Int64 ...
#   #
#   1   | 1      6   -1.83494  15.0        0          ...
#   2   | 2      9   -2.42858  19.1719     0          ...
#   3   | 3     12   -2.68342  23.3947     0          ...
#   4   | 4     19   -3.51728  30.5274     0          ...
#   :   | :     :       :       :       :       ...
# 9997 | 9997  48648 -7.79238  1.00169e5  329        48  ...
# 9998 | 9998  48399 -7.77228  99918.7   332        48  ...
# 9999 | 9999  48347 -7.76695  99855.1   331        48  ...
# 10000 | 10000 48231 -7.75921  99763.2   331        48  ...
#   6 columns and 9992 rows omitted
```

Here, we perform 10,000 steps of the FCIQMC algorithm. The target walker number, which determines the desired 1-norm of the vector, is set to 100,000. See Sec. 3 for more details on the FCIQMC algorithm.

The `DataFrame` holds time series of the various statistics `Rimu.jl` keeps track of. Of particular interest is the shift S , which is plotted in Fig. 1(a). It is used as a mechanism to control the norm of the FCIQMC vector, and also acts as an energy estimator. Initially, the shift fluctuates wildly, but then quickly settles to fluctuating around a fixed value. On the same time scale the one-norm of the FCIQMC vector grows and settles around the desired value of 10000 walkers as is shown in panel (b) of Fig. 1. The value the shift fluctuates around an estimator for the ground state energy of the Hamiltonian. For the estimate we discard the initial transient part of the time series and perform a blocked averaging procedure to extract the mean \bar{S} and its estimated statistical error $\sigma_{\bar{S}}$. These quantities are shown in Fig. 1 (c). There, we see that the true energy E_0 lies within the error bars given by the blocked average \bar{S} . See Sec. 4 for a detailed treatment of blocked averaging. In the code, we perform this averaging through the `shift_estimator` function.

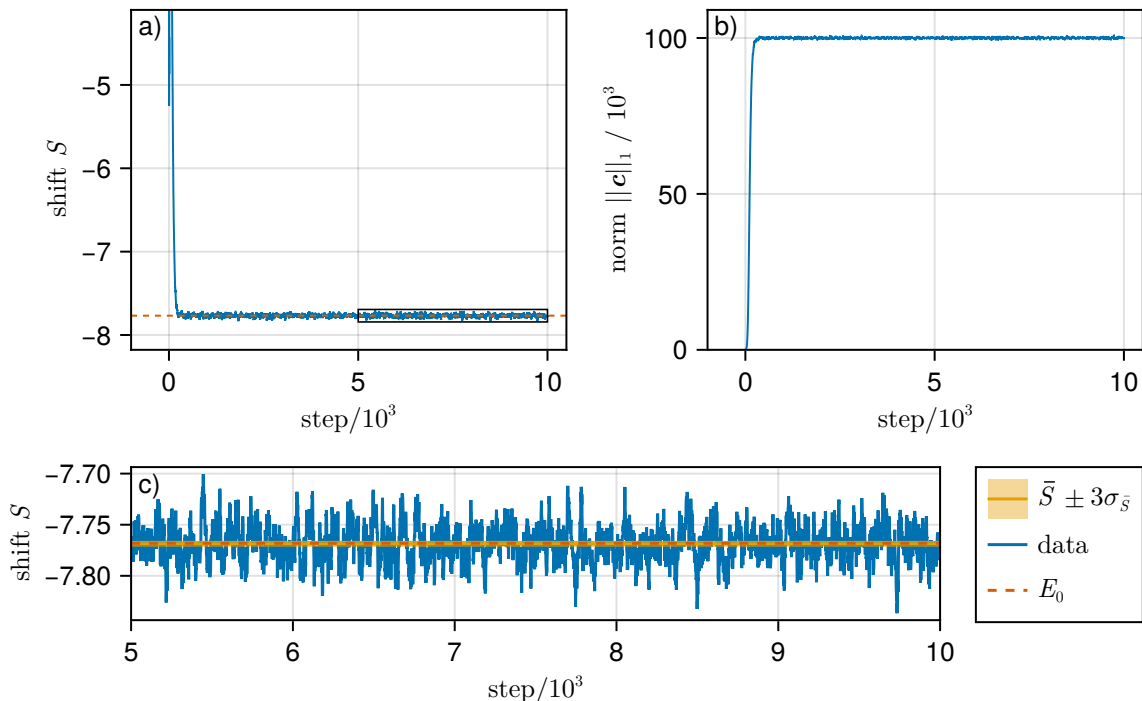


Figure 1: FCIQMC time series for the data obtained in the example. In panels (a) and (b), the shift and norm time series are shown. A close-up of the equilibrated region of the shift time series is shown in panel (c), which also shows the exact energy E_0 (dashed red line) and the estimate given by the mean of the shift \bar{S} (orange line) with a blocked standard error $\sigma_{\bar{S}}$ (orange band).

```
shift_estimator(df; skip=5000)
```

Here, `skip` sets the number of steps to be discarded from the beginning of the time series. Next, we extract the projected energy estimate by utilising the `projected_energy` function

```
projected_energy(df; skip=5000)
```

The values given by these functions are $\bar{S} = -7.76858 \pm 0.00075$ and $\bar{E}_y = -7.76809 \pm 0.00044$ for the shift and projected energy, respectively. These values compare favourably to the exact ground state energy $E_0 \approx -7.76815$ as obtained by exact diagonalisation (see Sec. 2.4).

2.2 Excited states

In addition to computing the ground state energy and properties, Rimu.jl also supports computing consecutive low-lying excited states. To do so, simply pass the parameter `n_spectral` to the `ProjectorMonteCarloProblem`.

```
problem_fciqmc_excited = ProjectorMonteCarloProblem(
    hamiltonian;
    last_step=10_000,
    target_walkers=100_000,
    post_step_strategy,
    n_spectral=2,
)
```

```
result = solve(problem_fciqmc_excited)
df = DataFrame(result)
```

Setting `n_spectral=2` triggers two independent step-synchronised FCIQMC simulations where the second's instantaneous coefficient vector is orthogonalised to the first one in order to target the first excited state. The resulting data frame now has a larger number of columns. For most of the statistics calculated, it contains columns postfixes with `_rls1` and `_rls2`, which correspond to the first and second spectral states for the first and only replica in this calculation. To get an estimate of the excited state energy, we again use the `shift_estimator` function, but now have to give it the name of the shift column from the data frame.

```
shift_estimator(df; shift=:shift_rls2, skip=5000)
```

The resulting value $\bar{S}_2 = -5.6646 \pm 0.0011$ matches the true excited state energy value of $E_1 \approx -5.6671$ well, which was obtained by exact diagonalisation. It should be noted, however, that computing excited state energies can be very difficult in practice as even in systems that are free of the Monte Carlo sign problem for ground state calculations, the sign problem always occurs for the excited states. Excited state calculations with Rimu.jl for the Fröhlich polaron model were reported in Ref. [14], where the sign problem could be mitigated by walker annihilation.

2.3 Observables

We now extend the example to compute observables - the density-density correlations defined by

$$\hat{G}^{(2)}(d) = \sum_i \hat{n}_i (\hat{n}_{i+d} - \delta_{d,0}) . \quad (2)$$

In Rimu.jl, both Hamiltonians and observables are operators and behave in a similar manner, which is reflected in a type hierarchy as explained in Sec. 6.2. We set up the computation as follows.

```
g2_operators = [G2RealCorrelator(d) for d in 0:6]
replica_strategy = AllOverlaps(g2_operators)

problem_fciqmc_observables = ProjectorMonteCarloProblem(
    hamiltonian;
    last_step=10_000,
    target_walkers=100_000,
    post_step_strategy,
    replica_strategy,
)

result = solve(problem_fciqmc_observables)

df = DataFrame(result)
```

Here, we first initialise a vector of observables with values of $d = 0, \dots, 6$ and then pass them into the `replica_strategy` `AllOverlaps`. The latter is a mechanism for computing overlaps between the FCIQMC vectors and observables after every Monte Carlo step. In order to compute those without bias, at least two independent runs of FCIQMC (replicas) must be run concurrently. The number of replicas can be specified, but two replicas are run by default when using `AllOverlaps`. See Sec. 4.3 for more information on calculating

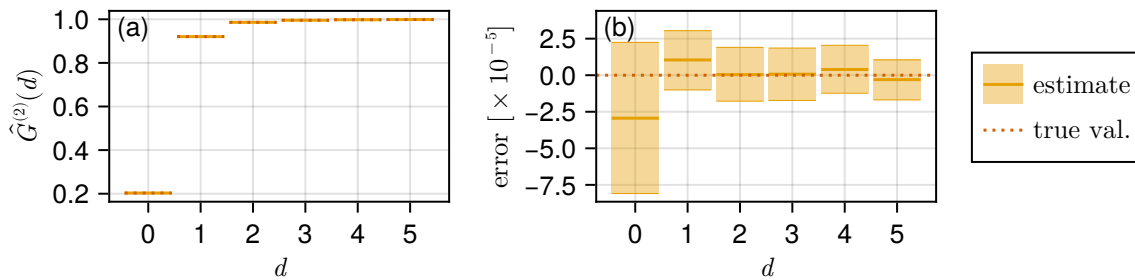


Figure 2: Estimates of the density-density correlator expectation values $\hat{G}^{(2)}(d)$ over a range of distances d . In panel (a), the orange bars show the estimates obtained from FCIQMC, where their widths are equal to 3 times the error bar. The exact values are plotted as dotted red lines. Panel (b) shows the error calculated from the differences between the estimates and the exact values.

observables with replicas. The resulting data frame now contains columns containing the dot-products between the vectors and each observable, which can be averaged with the `rayleigh_replica_estimator` function.

```
rayleigh_replica_estimator(result; op_name="Op1", skip=5000)
```

These estimates are compared to the exact values in Fig. 2. Computing observables with Rimu.jl’s FCIQMC was used to compute density-density correlations of an impurity in a one-dimensional interacting Bose gase in Ref. [17].

2.4 Exact diagonalisation

Because our example is small enough, we can confirm the correctness of the FCIQMC result by performing exact diagonalisation of the Hamiltonian and comparing the exact and numerical results for the energy. Rimu.jl is compatible with eigenvalue solvers from several external packages, as discussed in Sec. 5. Here, we use the KrylovKit [39] package. The interface is similar to the one used for FCIQMC — we first define a problem by instantiating an `ExactDiagonalizationProblem` which we then solve with the `solve` function.

```
using KrylovKit

problem = ExactDiagonalizationProblem(
    hamiltonian; algorithm=KrylovKitSolver(false),
)
exact_result = solve(problem)
```

The exact energies can then be extracted by accessing

```
exact_result.values
```

while the eigenvectors are stored in

```
exact_result.vectors
```

Exact diagonalisation of transcorrelated [40] Hamiltonians with Rimu.jl was used to solve one-dimensional few-fermion and impurity problems in Refs. [16, 41].

This example shows the basics of Rimu.jl's usage in a small system. Rimu.jl can be used in a similar manner with many other types of Hamiltonians and both its FCIQMC and exact diagonalisation capabilities can be scaled up to much larger problems. As an example, Rimu.jl was used in Ref. [15] to compute the ground state of a two-dimensional impurity-Bose-Hubbard Hamiltonian with 100 particles on 100 sites, which has a Hilbert space dimension of $\sim 4.5 \times 10^{60}$. As the computational effort grows with system size and complexity of the problem so does the demand for computational resources. Rimu.jl has extensive capabilities for leveraging both multi-core parallelism and multi-node distributed computing. The core implementation strategies are discussed in Sec. 6.4 and scaling benchmarks on a high-performance computing facility presented in Sec. 7.

3 The FCIQMC algorithm

Full configuration interaction quantum Monte Carlo (FCIQMC) is an algorithm for stochastically sampling the lowest eigenpair (E_0, \mathbf{v}_0) of a linear operator \hat{H} . Since we are dealing with finite systems, \hat{H} can be represented as a matrix but as we will discuss later, there is no need to store the actual matrix in memory. How operators and vectors are implemented in the code is discussed in more detail in Secs. 6.2 and 6.3.

3.1 A fixed point iteration

FCIQMC belongs to the wider class of projector Monte Carlo methods. These methods work by discretising the imaginary-time Schrödinger equation

$$\frac{\partial |\Psi(\tau)\rangle}{\partial \tau} = -\hat{H} |\Psi(\tau)\rangle, \quad (3)$$

and then solving the discretised equation stochastically. In the case of FCIQMC, the discretisation employed is an Euler method

$$|\Psi(\tau + \delta\tau)\rangle = |\Psi(\tau)\rangle - \delta\tau \hat{H} |\Psi(\tau)\rangle, \quad (4)$$

where $\delta\tau$ is a (small) imaginary time step.

Since we are interested in solving the equation numerically, we realise \hat{H} as a matrix \mathbf{H} with entries

$$H_{i,j} = \langle i | \hat{H} | j \rangle \quad (5)$$

where i, j are (not necessarily integer) indices and $|i\rangle, |j\rangle$ are basis states. Similarly, we realise the state $|\Psi(n \delta\tau)\rangle$ as a coefficient vector $\mathbf{c}^{(n)}$ with coefficients

$$c_i^{(n)} = \langle i | \Psi(n \delta\tau) \rangle. \quad (6)$$

We use $\mathbf{c}^{(0)}$ to denote the starting vector. Then, Eq (4) can be converted to

$$\mathbf{c}^{(n+1)} = \mathbf{T}^{(n)} \mathbf{c}^{(n)}, \quad (7)$$

where \mathbf{T} is the FCIQMC transition operator

$$\mathbf{T}^{(n)} := \mathbf{1} + \delta\tau \left(S^{(n)} \mathbf{1} - \mathbf{H} \right). \quad (8)$$

Here, $\mathbf{1}$ is the identity matrix and $S^{(n)}$ is an energy *shift*. If the shift is held constant, the scheme admits exponential solutions, where the norm of \mathbf{c} grows or decays exponentially, with $S^{(n)} = E_0$ being the only stable solution. Hence, Eq. (7) presents an unstable fixed-point iteration scheme on \mathbf{c} with a fixed point at the desired eigenpair $\mathbf{c} = \mathbf{v}_0$ and $S = E_0$.

To stabilise the fixed point, we update the value of $S^{(n)}$ after every step with the following procedure

$$S^{(n+1)} = S^{(n)} - \frac{\zeta}{\delta\tau} \ln \frac{\|\mathbf{c}^{(n+1)}\|_1}{\|\mathbf{c}^{(n)}\|_1} - \frac{\xi}{\delta\tau} \ln \frac{\|\mathbf{c}^{(n+1)}\|_1}{N_t}, \quad (9)$$

where N_t is the target 1-norm of the coefficient vector and ζ and ξ are parameters controlling the dynamics of the shift. It was shown in Ref. [42] that the combination of Eq. (7) with the shift update of Eq. (9) behaves like a (discretised) damped harmonic oscillator differential equation for the logarithmic 1-norm of the vector. In this interpretation of the equation, the terms with parameters ζ and ξ represent the damping and forcing terms, respectively. The combination of Eqs. (7) and (9) presents a stable fixed-point iteration scheme on the pair $(S^{(n)}, \mathbf{c}^{(n)})$ with a fixed point at the eigenpair (E_0, \mathbf{v}_0) with a normalized eigenvector $\|\mathbf{v}_0\|_1 = N_t$.

An advantage of FCIQMC over some other methods is that it has no time step error. This can be seen from the fact that $\delta\tau$ does not play a role in determining the values of the fixed points. However, the choice of $\delta\tau$ is still important, as the algorithm will only converge if

$$\delta\tau < \frac{2}{E_{\max} - E_0}, \quad (10)$$

where E_{\max} is the largest eigenvalue of \mathbf{H} and $E_{\max} - E_0$ is its spectral range [43].

As demonstrated in Sec. 2.2, FCIQMC can be extended to compute low-lying excited states in addition to the ground state. To compute the first K states, we run FCIQMC in parallel on K independent vectors $\mathbf{c}^{(n,k)}$, $k = 0, \dots, K - 1$ with independent shifts $S^{(n,k)}$. Then after every step, we orthogonalise the vectors using the Gram-Schmidt procedure, which ensures each vector converges to a separate spectral state \mathbf{v}_k , while each shift converges to the energy of that state E_k [28].

3.2 Quantum Monte Carlo

The method described thus far is equivalent to the power method with a different normalization scheme and as such provides no benefits over standard methods for eigenvalue computation. However, unlike many other methods, it can be performed stochastically by replacing the operator \mathbf{T} with a stochastic operator $\check{\mathbf{T}}$. For this to be beneficial, we pick $\check{\mathbf{T}}$ in a way that reduces the computational cost of the operator application in Eq. (7). At the same time, we must ensure that the fixed points of Eqs. (7) and (9) remain unchanged. To achieve this, we require the stochastic operator to be equal to the deterministic operator in expectation:

$$\mathbb{E} [\check{\mathbf{T}}^{(n)} \mathbf{c}^{(n)}] = \mathbf{T}^{(n)} \mathbf{c}^{(n)}, \quad (11)$$

where \mathbb{E} denotes the ensemble average.

Because applying $\check{\mathbf{T}}$ is noisy, the algorithm does not cleanly converge to (E_0, \mathbf{v}_0) . Instead, the output is a time series with two phases; an equilibration phase, where the algorithm moves $S^{(n)}$ and $\mathbf{c}^{(n)}$ towards the desired fixed points, and a phase where the algorithm has reached the fixed point and is fluctuating around it. To extract an estimate of E_0 from the algorithm, we discard all shift data from the first phase and take an average of the second. An example of an FCIQMC time series is shown in Fig. 1.

Rimu.jl provides several ways of realising the stochastic operator $\tilde{\mathbf{T}}$. In this section, we describe the one we have found to be the most useful. Further details of the algorithm and how they affect the computation are presented in Sec. 3.2. Although the algorithm was originally formulated in Monte Carlo terminology with walkers who spawn, die, and annihilate [9], here we describe the procedures in terms of *matrix compression* and *vector compression* [26].

To start, we write a coefficient vector \mathbf{c} as

$$\mathbf{c} = \sum_i c_i \hat{\mathbf{i}}. \quad (12)$$

Here, we can call the orthonormal set of vectors $\{\hat{\mathbf{i}}\}_i$ the primitive basis indexed by the addresses i . In our case, these addresses are Fock states. A matrix-vector product can then be seen as

$$\mathbf{T} \mathbf{c} = \sum_i \mathbf{T}_{:,i} c_i, \quad (13)$$

where $\mathbf{T}_{:,i}$ represents the i -th column of \mathbf{T} . In a Monte Carlo inspired view, the process in Eq. (13) can be seen as each entry in \mathbf{c} independently spawning $\mathbf{T}_{:,i} c_i$. These spawns are then collected and summed together. This summing is often referred to as walker annihilation and is a critical step that allows FCIQMC to overcome the sign problem through cancellation of positive and negative contributions to a vector [9].

We convert the matrix \mathbf{T} to a stochastically compressed operator $\tilde{\mathbf{T}}$ in two distinct phases, the first of which is matrix compression. Matrix compression replaces the spawning step from Eq. (13) with a stochastic procedure that avoids visiting some elements of \mathbf{T} . The matrix-compressed operator is denoted as $\tilde{\mathbf{T}}$. Suppose we are spawning the column corresponding to the coefficient c_i , and that the column $\mathbf{T}_{:,i}$ contains m_i non-zero off-diagonal elements. We start by determining the number of spawning attempts

$$n_i = \lceil |c_i| \rceil. \quad (14)$$

where $\lceil x \rceil$ denotes the smallest integer greater than or equal to x . Next, we pick n_i non-zero off-diagonal elements from the column uniformly at random with replacement. This allows us to construct a stochastically compressed column

$$\tilde{\mathbf{T}}_{:,i} = \left(\tilde{T}_{j,i} \right)_j \quad (15)$$

where

$$\tilde{T}_{j,i} = \begin{cases} T_{i,i} & \text{if } j = i \\ \frac{m_i}{n_i} T_{j,i} & \text{if } j \text{ was selected in the picking step,} \\ 0 & \text{otherwise.} \end{cases} \quad (16)$$

If the requested number of spawns is greater than m_i , we set $\tilde{\mathbf{T}}_{:,i} = \mathbf{T}_{:,i}$, *i.e.*, no stochastic compression takes place and the spawning step is executed exactly. This results in a semistochastic algorithm similar to the one described in Ref. [18] and is discussed in more detail in Sec. 7.1. The factor of m_i/n_i in Eq. (16) represents the inverse probability of picking the element. The result is scaled by it so that $\mathbb{E}[\tilde{T}_{j,i}] = T_{j,i}$ holds. Note that this procedure always leaves the diagonal element $T_{i,i}$ unchanged, and if the coefficient c_i is high enough, the column remains uncompressed.

The other building block in the compression scheme is stochastic vector compression. The goal here is to reduce the number of non-zero values in the coefficient vector \mathbf{c} without

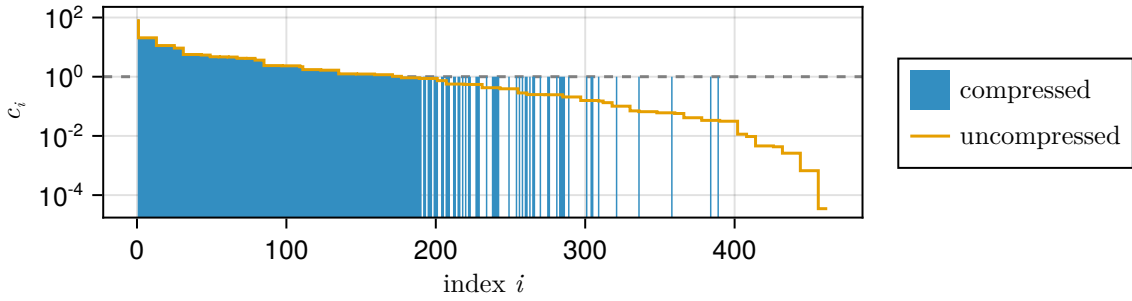


Figure 3: Stochastic vector compression. The plot shows the values c_i at a given index i of an uncompressed vector (yellow line) with a stochastically compressed vector (blue fill) superimposed on it. In the compressed vector, the coefficients with value $c_i \geq 1$ are unaffected by compression, while those below 1 are stochastically set to either 0 or 1 with probability proportional to c_i .

changing the vector in expectation. This is done by applying a stochastic projection scheme $\check{\Pi}$, which is defined as follows:

$$(\check{\Pi}\mathbf{c})_i = \begin{cases} c_i & \text{if } c_i \geq 1, \\ 1 & \text{if } c_i < 1 \text{ with probability } c_i, \\ 0 & \text{if } c_i < 1 \text{ with probability } 1 - c_i. \end{cases} \quad (17)$$

Similarly to the matrix compression scheme described above, this procedure has the property that increasing the 1-norm of the vector \mathbf{c} lessens the effect $\check{\Pi}$ has on it. A plot showing an example of a vector compressed this way is shown in Fig. 3. The figure shows the ground state eigenvector of the real space Bose-Hubbard Hamiltonian with $N = 6$ particles in $M = 6$ sites with an interaction strength of $u/t = 6$, which was normalized such that $\|\mathbf{c}\|_1 = 1000$.

Finally, we combine matrix compression and vector compression to realise the stochastically compressed operator $\check{\mathbf{T}}$, defined by

$$\check{\mathbf{T}}\mathbf{c} = \check{\Pi} \left(\sum_i \check{\mathbf{T}}_{:,i} c_i \right). \quad (18)$$

Using the compressed operator $\check{\mathbf{T}}$ in place of \mathbf{T} reduces the computational cost of a single matrix-vector multiplication considerably. When there is a small region in the vector where the coefficients c_i are high, with the rest of the vector very close to zero, the vector compression scheme leaves the localised region mostly intact, while heavily compressing the (less important) low-valued regions. Matrix compression also ensures that the spawns from important, high-valued regions of the vector are performed essentially exactly, while the spawns from the low-valued regions of the vector are performed in a noisy manner. A consequence of this is that FCIQMC works best when the ground state eigenvector of \mathbf{H} is extremely localised. Where possible, the basis should be chosen so that the ground state is localised in Fock space.

When using the stochastic algorithm, the target norm N_t in Eq. (9) plays an important role. By increasing N_t , the stochastic operation $\check{\mathbf{T}}^{(n)}\mathbf{c}^{(n)}$ tends towards its exact counterpart, $\mathbf{T}^{(n)}\mathbf{c}^{(n)}$. Thus, simulations with higher N_t will be less noisy, giving better eigenvalue estimates, but be computationally more intensive. Setting a higher N_t also helps mitigate two issues present in stochastic FCIQMC, namely the population control bias and the sign problem. The population control bias, which is always present, is discussed in-depth in

Ref. [44]. It becomes apparent when the compressed vector is much smaller than the size of the full address set and is related to the noise in the algorithm. Several methods of mitigating it are available in Rimu.jl, as described in Secs. 4.2 and 6.2. The other issue is the sign problem, which presents itself in Hamiltonians with positive off-diagonal elements. When the compressed vector representation is too small to fully capture the sign structure of the true eigenvector, FCIQMC converges to the wrong eigenpair [43]. It can be overcome by using a N_t above a critical value N_c , or be traded for an (often small) bias with the initiator approximation [19].

4 Computing observables

The main output of an FCIQMC simulation in Rimu.jl are the time series of several quantities. By default, at each step the algorithm will record the value of the shift $S^{(n)}$, the vector norm $\|\mathbf{c}^{(n)}\|_1$ and several diagnostic quantities. Additional observables can be calculated during the simulation in which case time series of vector-vector and vector-operator-vector products will also be reported. The `StatsTools` module in Rimu.jl contains a range of functions for calculating observables from the time series after an FCIQMC simulation. Many of the convenience functions in the `StatsTools` module are specific to analysis for the FCIQMC algorithm and the typical Hamiltonian models studied, but the underlying functionality is flexible and extensible.

For this section, we will refer to a simple problem using the one-dimensional Bose-Hubbard Hamiltonian of 6 particles in 6 lattice sites.

```
julia> initial_address = near_uniform(BoseFS{6,6});
julia> H = HubbardRealSpace(initial_address; u = 6.0);
```

The implementation of Fock addresses and Hamiltonians is explained in Section 6. For now, we perform the simulation for 3000 time steps.

```
julia> last_step = 3000;
julia> problem = ProjectorMonteCarloProblem(H; last_step);
julia> df = DataFrame(solve(problem));
```

The output `df` is a `DataFrame` [38] whose columns are the time series of the quantities produced during the FCIQMC simulation. In the following sections, we will describe how the time series are analysed to produce physically meaningful observables.

4.1 Time-series analysis

Even after equilibration, consecutive time steps of a QMC simulation are correlated, and the data must be decorrelated to obtain accurate estimates. For a general stationary time series quantity X , assuming ergodicity, the expected value $\langle X \rangle$ is the long-time limit of the sample mean

$$\langle X \rangle = \lim_{\Omega \rightarrow \infty} \overline{X}, \quad (19)$$

where

$$\overline{X} = \frac{1}{\Omega} \sum_{n=1}^{\Omega} X^{(n)}, \quad (20)$$

is the sample mean of a time series with Ω time steps. A quantity of primary interest is the variance of the sample mean defined by

$$\sigma_{\bar{X}}^2 = \langle \bar{X}^2 \rangle - \langle \bar{X} \rangle^2, \quad (21)$$

and the related standard error $\sigma_{\bar{X}}$. This standard error quantifies the statistical uncertainty we have about the position of the expected value, given a sample mean calculated from a finite time series. Estimating the variance $\sigma_{\bar{X}}^2$ from a given time series is complicated by the fact that nearby elements of the time series will typically be strongly correlated in a QMC calculation, *e.g.* due to the fact that only a small step is performed in each iteration.

The main method in Rimu.jl to remove correlations from time series uses the so-called blocking analysis [45]. The variance of the sample mean can be expressed as

$$\sigma_{\bar{X}}^2 = \frac{\gamma_0}{\Omega} + \frac{2}{\Omega} \sum_{t=1}^{\Omega-1} \left(1 - \frac{t}{\Omega}\right) \gamma_t, \quad (22)$$

where $\gamma_t = \langle X^{(i)} X^{(j)} \rangle - \langle X^{(i)} \rangle \langle X^{(j)} \rangle$ expresses the (unknown) correlation function of the time series, which is expected to only depend on the difference $t = |i - j|$. The blocking analysis works by transforming the time series iteratively, and reducing its correlations, by re-blocking the data. At each iteration a new time series X' is built from ‘blocks’ which are the average of consecutive steps

$$X'^{(i)} = \frac{1}{2} \left(X^{(2i-1)} + X^{(2i)} \right). \quad (23)$$

The new time series has length $\Omega' = \Omega/2$ while the sample mean $\bar{X}' = \bar{X}$ and variance $\sigma_{\bar{X}'}^2 = \sigma_{\bar{X}}^2$ are unchanged. However, the correlation functions are altered (and reduced) by the transformation Eq. (23) such that at each iteration the leading-order term γ'_0/Ω increases while the higher-order terms $t > 0$ decrease. After some number of iterations the size of the blocks will exceed the correlation time scale of the original data and the blocks will be uncorrelated. At this point the leading-order term in Eq. (22) will plateau (within random fluctuations) and higher-order terms will be negligible so that $\sigma_{\bar{X}}^2 \approx \gamma'_0/\Omega$ is a good estimate. The blocking analysis also provides an estimate of the uncertainty in $\sigma_{\bar{X}}^2$ and in practice this uncertainty in $\sigma_{\bar{X}}^2$ rises after the estimates for $\sigma_{\bar{X}}^2$ have plateaued. The detection of this plateau and the minimum number of blocking iterations to achieve it are automated with the M -test [46], which detects when the higher-order correlations, in particular γ_1 , are indistinguishable from zero at a specified confidence level.

In Rimu.jl the blocking analysis is provided by the `blocking_analysis` function in the `StatsTools` module that can be applied to a time series:

```
julia> correlated_ts = smoothen(randn(10_000), 128);

julia> blocking_analysis(correlated_ts)
BlockingResult{Float64}
mean = -0.0027 ± 0.0095
with uncertainty of ± 0.0007686451776019342
from 78 blocks after 7 transformations (k = 8).
```

See Fig. 4 for a graphical depiction of the M -test performed on this data.

4.2 Energy estimators

The simplest observable that can be calculated in an FCIQMC calculation is the expectation value of the shift $\langle S \rangle$, which is an estimator of the ground state energy. The update

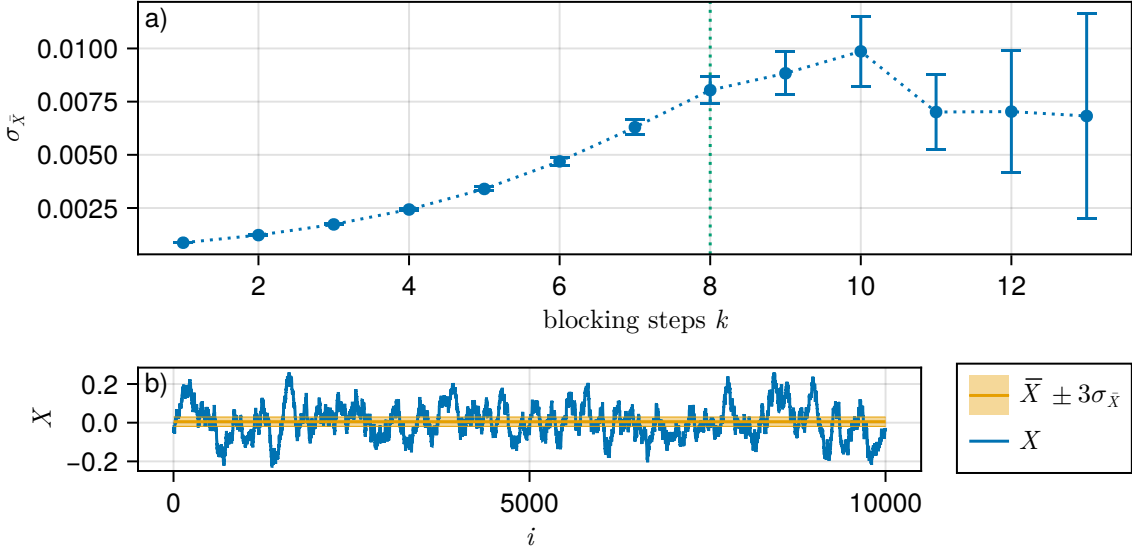


Figure 4: The M -test performed on points of synthetic data. Panel a) shows how the standard error $\sigma_{\bar{X}}$ changes as the number of blocking steps k increases. Note that past $k = 8$, the values of $\sigma_{\bar{X}}$ are equivalent up to their error bars, hence the M -test identifies $k = 8$ as the appropriate level of blocking. The bottom panel b) shows the raw data with the calculated mean and blocked standard error superimposed on it.

procedure Eq. (9) means that the shift behaves as a critically damped harmonic oscillator on average. After the initial equilibration phase $S^{(n)}$ is a stationary time series fluctuating about the expected value $\langle S \rangle$. Blocking analysis is sufficient to decorrelate the data and obtain an energy estimator using the shift time series $S^{(n)}$. This is the most common analysis for FCIQMC so `StatsTools` has a convenience function called `shift_estimator` for performing the blocking analysis on the output of a simulation. This function automatically extracts the correct column from the output `DataFrame` and performs a blocking analysis on the time series. For the output `df` of solving the `ProjectorMonteCarlo` from the start of this section we have

```
julia> shift_estimator(df; skip = 1_000)
BlockingResult{Float64}
mean = -4.0225 ± 0.0034
with uncertainty of ± 0.00021708770311760708
from 125 blocks after 4 transformations (k = 5).
```

Note the keyword argument to skip the first steps and avoid the equilibration phase.

While the shift estimator $\langle S \rangle$ is the easiest to calculate, there are other useful estimators of the ground state energy, such as the projected energy

$$\bar{E}_y = \frac{\langle \mathbf{y}^\dagger \mathbf{H} \mathbf{c} \rangle}{\langle \mathbf{y}^\dagger \mathbf{c} \rangle}, \quad (24)$$

where \mathbf{y} is a fixed reference vector. Different choices of \mathbf{y} yield different energy estimators or provide relations to estimate the population control bias [44]. A useful example is the norm-projected energy where $\mathbf{y} = \tilde{\mathbf{1}}$, which is a vector whose components have unit magnitude and match the sign of the ground state eigenvector \mathbf{v}_0 . Another is the variational energy E_{var} with $\mathbf{y} = \langle \mathbf{c} \rangle$. In addition to being estimators of the ground state energy, these

quantities are practical since in each case Eq. (24) is computable at each step from the instantaneous vector and the Hamiltonian. For details see Ref. [44]. In any case, the estimator Eq. (24) is obtained in two steps. First, for each time step, after spawning and annihilation is finished the (compressed approximation of the) instantaneous vector $\mathbf{c}^{(n)}$ and the Hamiltonian are used to separately calculate the numerator and denominator of Eq. (24) as two time series. Second, the two output time series should be combined to obtain \bar{E}_y . This estimator is therefore a ratio of fluctuating quantities and propagation of uncertainty must be performed carefully, particularly when the denominator may be near zero due to fluctuations.

For a quantity of interest $\langle X/Y \rangle$ defined by two time series X and Y the sample means \bar{X} and \bar{Y} define the mean value of the ratio $r = \bar{X}/\bar{Y}$. To estimate the error σ_r on this ratio, first estimate σ_X and σ_Y , either from the sample variances $\sigma_X^2 = \text{var}(X)$ and $\sigma_Y^2 = \text{var}(Y)$, or better yet, from the blocking analysis on each time series separately. These values and the covariance $\rho = \text{cov}(X, Y)$ define a correlated normal distribution of the ratio. This distribution is sampled using Monte Carlo methods provided by the `MonteCarloMeasurements.jl` [47] package to determine the error σ_r on the ratio of means $r = \bar{X}/\bar{Y}$.

The calculation of ratio estimators is provided by the function `ratio_of_means` in the `StatsTools` module.

```
julia> Xs = 2 .+ smoothen(randn(10_000), 128);
julia> Ys = 1 .+ smoothen(randn(10_000), 64);

julia> ratio_of_means(Xs, Ys)
RatioBlockingResult{Float64, MonteCarloMeasurements.Particles{Float64, 2000}}
ratio = 1.96085 ± (0.0205071, 0.0179696) (MC)
95% confidence interval: [1.92504, 2.00045] (MC)
linear error propagation: 1.96205 ± 0.0193621
|δ_y| = |0.00868362| (< 0.1 for normal approx)
Blocking successful with 78 blocks after 7 transformations (k = 8).
```

The output is a `RatioBlockingResult` which contains information about the ratio distribution. In order for this method to work the ratio distribution should be normally distributed which is a good approximation if the parameter $\delta_Y = \sigma_Y/\bar{Y}$ is small (typically $\lesssim 0.1$).

To calculate a projected energy during an FCIQMC simulation, first define a post-step strategy which indicates how to use existing information to calculate additional quantities when solved. For example, we could choose the fixed reference vector to be the initial vector $\mathbf{y} = (N_w, 0, \dots)$, where N_w is the initial number of walkers at the start of the simulation, (by default $N_w = 10$). That is, all walkers start on the initial Fock address, and all other Fock addresses have zero walkers initially.

```
julia> initial_vector = default_starting_vector(H);
julia> post_step_strategy = ProjectedEnergy(H, initial_vector);
```

Then the simulation is re-run with this post-step strategy

```
julia> problem = ProjectorMonteCarloProblem(H; last_step, post_step_strategy);
julia> df = DataFrame(solve(problem));
```

The `StatsTools` module provides a convenience function `projected_energy` that automatically extracts the correct time series from the output and calculates the ratio of

means.

```
julia> projected_energy(df; skip = 1_000)
RatioBlockingResult{Float64, MonteCarloMeasurements.Particles{Float64, 2000}}
ratio = -4.02064 ± (0.00195644, 0.00216691) (MC)
95% confidence interval: [-4.02469, -4.01672] (MC)
linear error propagation: -4.02066 ± 0.00205069
|δ_y| = |0.000765156| (≤ 0.1 for normal approx)
Blocking successful with 62 blocks after 5 transformations (k = 6).
```

The `StatsTools` module provides other convenience functions for energy estimators such as `variational_energy_estimator` for calculating the variational energy, but this estimator requires that the simulation is run with more than one replica, explained in the next section.

4.3 General observables

In addition to estimators of the ground state energy, `Rimu.jl` is able to calculate general observables. Since the instantaneous vectors are unnormalised we wish to calculate expected values of a general operator \hat{Q} as a Rayleigh quotient

$$\langle \hat{Q} \rangle = \frac{\langle \mathbf{c}^\dagger \mathbf{Q} \mathbf{c} \rangle}{\langle \mathbf{c}^\dagger \mathbf{c} \rangle}. \quad (25)$$

The implementation of the matrix representation \mathbf{Q} will be discussed in Section 6.2. The Rayleigh quotient also depends on the state vector \mathbf{c} which will of course be approximated during a Monte Carlo simulation. However, even keeping an estimate of the entire (*i.e.*, uncompressed) vector can be computationally prohibitive when the Hilbert space scales exponentially. Instead, here we discuss how the numerator and denominator of Eq. (25) are computed via the replica trick, using multiple independent simulations. For further details and demonstration of the effectiveness of this technique see Ref. [44].

In `Rimu.jl` an FCIQMC simulation can be run with R instances, or replicas, to be run simultaneously and independently. At each time step, the FCIQMC algorithm propagates vectors \mathbf{c}_A , $A = 1, \dots, R$. They are statistically independent in that $\text{cov}(\mathbf{c}_A, \mathbf{c}_B) = 0$ but model the same system *i.e.*, $\langle \mathbf{c}_A \rangle = \langle \mathbf{c}_B \rangle = \mathbf{v}_0$. For each pair of replicas (A, B) we calculate the vector-vector dot-product $\mathbf{c}_A^{(n)\dagger} \mathbf{c}_B^{(n)}$ and vector-operator-vector dot-product $\mathbf{c}_A^{(n)\dagger} \mathbf{Q} \mathbf{c}_B^{(n)}$. These products are reported as time series so that the expected value $\langle \hat{Q} \rangle$ is then estimated as

$$\bar{Q} = \frac{\sum_{(A,B)}^R \overline{\mathbf{c}_A^\dagger \mathbf{Q} \mathbf{c}_B}}{\sum_{(A,B)}^R \overline{\mathbf{c}_A^\dagger \mathbf{c}_B}}, \quad (26)$$

where the sample means $\bar{\cdot}$ in the numerator and denominator are obtained with the blocking analysis discussed in Section 4.1 and the overall estimator for \bar{Q} is obtained with the ratio estimator discussed in Section 4.2.

From Eq. (26) it is necessary to use at least two replicas and it can be beneficial to use more. Due to random fluctuations and sparseness of the vectors \mathbf{c}_A the vector-vector product for any one pair may be sampled close to zero. Using more than two replicas reduces the variance in the overall denominator of Eq. (26), which scales as $1/\sqrt{R(R-1)\Omega}$, and thus the ratio estimator \bar{Q} also has smaller variance. However, the computational cost of R replicas each running for Ω time steps scales as $R\Omega$ and the cost of computing dot products between replicas scales as R^2 . In practice, we find that $R = 2, 3$ or 4 is sufficient in most cases for greatly improving the statistics of general observables without ballooning computational cost.

For the simple Bose-Hubbard example in Sec. 2, we could calculate the two-body correlation function

$$\hat{G}^{(2)}(d) = \frac{1}{M} \sum_i^M \hat{n}_i(\hat{n}_{i+d} - \delta_{0d}) \quad (27)$$

where d is the interparticle-separation, M is the number of lattice sites and \hat{n}_i is the number operator for lattice site i . First, the operators are defined in Rimu.jl for a few values of d

```
julia> d_values = 0:2
julia> G2list = ((G2RealCorrelator(d) for d in d_values)...);
```

See Section 6.2 for how the operators are implemented. Next, a `ReplicaStrategy` is defined to run the simulation with two replicas:

```
julia> n_replicas = 2;
julia> replica_strategy = AllOverlaps(n_replicas; operator = G2list);
julia> problem = ProjectorMonteCarloProblem(H; last_step, replica_strategy);
julia> df = DataFrame(solve(problem));
```

`AllOverlaps` is a `ReplicaStrategy` that indicates that vector-vector and vector-operator-vector overlaps should be calculated between all pairs of replicas at each time step. Estimates for the two-body correlations are extracted from the output `df` with the convenience function `rayleigh_replica_estimator`:

```
julia> for d in d_values
    r = rayleigh_replica_estimator(df; op_name = "Op$(d+1)", skip = 1_000);
    println("G2($d) = ", (r.f), " ± ", (r.σ_f))
end
G2(0) = 0.21506270309323064 ± 8.084576238283286e-5
G2(1) = 0.9164162344704037 ± 3.322465208050791e-5
G2(2) = 0.981605515982267 ± 4.056637600473594e-5
```

Note that the default column names for operator overlaps are 1-indexed but the d values start at zero. This example began with a state with unit filling and high interparticle interaction strength, so we see that the onsite correlation is low and correlations for $d > 0$ are close to 1, consistent with the Mott insulating phase of the Bose-Hubbard model.

Apart from defining additional operators for calculating observables, replicas are also useful for energy estimators discussed in Section 4.2. For energy estimators that can be obtained from a single replica, such as the norm-projected energy, time series are calculated for each replica independently, providing more data. For the variational energy estimator E_{var} where the reference vector is the instantaneous vector $\mathbf{y} = \langle \mathbf{c} \rangle$ it is not feasible to store \mathbf{c} at every step during the simulation. Instead, E_{var} is obtained by using the average of the shifts, i.e. $\mathbf{c}_A^\dagger \mathbf{Q} \mathbf{c}_B = \frac{1}{2}(S_A + S_B) \mathbf{c}_A^\dagger \mathbf{c}_B$ for each pair of replicas in (26). The convenience function `variational_energy_estimator` combines the shift time series from all replicas to produce a ratio of means.

```
julia> variational_energy_estimator(df; skip = 1_000)
RatioBlockingResult{Float64, MonteCarloMeasurements.Particles{Float64, 2000}}
ratio = -4.02149 ± (0.00248037, 0.00245498) (MC)
95% confidence interval: [-4.02635, -4.01664] (MC)
linear error propagation: -4.02163 ± 0.00248588
|δ_y| = |0.000943422| (≤ 0.1 for normal approx)
Blocking successful with 62 blocks after 5 transformations (k = 6).
```

Without multiple replicas `variational_energy_estimator` will error.

Because this example is for a small system all three energy estimators obtain similar estimates of the ground state energy $E = -4.02$. For more realistic problems where the Hilbert space is much larger than the number of walkers and the population control bias can be significant, it is useful to have different estimators for estimating the ground state energy. Typically, the variational energy estimator is nominally the best, but it requires multiple replicas and is thus the most expensive to calculate. The projected energy estimator is simpler to calculate, but is not useful when the sign problem is significant. The shift estimator is also easy to calculate but typically has a larger population control bias. Which one is best depends on the problem and the available resources .

4.4 Reweighting

Finally, we briefly mention an advanced technique for analysing the time series produced by FCIQMC simulations. As mentioned in Sec. 3.2, the population control bias is always present when the size of the Hilbert space is much larger than the number of walkers. Methods for dealing with the population control bias in FCIQMC are discussed in detail in Ref. [44], including a procedure called reweighting, which is based on the methods of Ref. [21]. The idea is to consider an idealised FCIQMC procedure for a different coefficient vector $\mathbf{f}^{(n)}$ where the fluctuating shift $S^{(n)}$ is replaced by a constant reference energy in Eq. (8). The reference energy is arbitrary but in principle can be chosen so that the population control bias is formally eliminated. In practice such a procedure would be exponentially unstable, but $\mathbf{f}^{(n)}$ can be approximated by a transformation of the usual coefficient vector $\mathbf{f}^{(n)} = w_h^{(n)} \mathbf{c}^{(n)}$. The weights $w_h^{(n)}$ are designed to counter the effect of fluctuations in the shift $S^{(n)}$, thus reducing the population control bias. The parameter h controls the window over which the time series is altered. Importantly, the reweighting procedure is not actually applied to the coefficient vector $\mathbf{c}^{(n)}$ during the simulation and instead the output time series of an ordinary FCIQMC simulation are adjusted by the weights $w_h^{(n)}$. In principle, energy estimators can be constructed from reweighted time series that are asymptotically unbiased as $h \rightarrow \infty$ and $\delta\tau \rightarrow 0$. In practice the variance grows as h becomes large, but for small h there can be an improvement in the population control bias. The efficacy of the reweighting procedure for FCIQMC is explored more thoroughly in Ref. [44]. Here we remark that the `StatsTools` module contains convenience functions `mixed_estimator` and `growth_estimator` to calculate energy estimators using the reweighting technique, and `rayleigh_replica_estimator` can also use reweighting to reduce the effect of the population control bias on estimates of observables.

5 Exact diagonalisation

While the main focus of Rimu.jl is quantum Monte Carlo, it also supports exact diagonalisation through wrappers to KrylovKit.jl [39], Arpack.jl [48,49], and IterativeSolvers.jl [50]. The diagonalisation can be performed in two ways — through explicitly building a sparse matrix, and through matrix-free methods. Both methods are exposed to the user through an interface based on CommonSolve.jl [37].

The sparse matrix methods are straightforward; the Hamiltonian is converted to a matrix and passed to the solver. To convert an operator to a sparse matrix, we treat it as a graph whose vertices correspond to the basis elements and its edges correspond to non-zero off-diagonal elements of the operator. We then walk the graph in a parallel breadth-first search and record all encountered off-diagonal elements in a list that is later

converted to a matrix. Converting a Hamiltonian to a matrix is only feasible with small problems, as the matrices quickly grow too large to store in memory, even if they are sparse.

For use with matrix-free methods, the Hamiltonian is wrapped in a way that follows the interface from `LinearMaps.jl` [51]. This allows us to multiply the Hamiltonian with a standard Julia vector much like one would a `Matrix`. An operator–vector product $\mathbf{w} = \mathbf{H}\mathbf{v}$ is then executed by calculating each element of \mathbf{w} as

$$w_i = \mathbf{H}_{i,:}\mathbf{v}, \quad (28)$$

where $\mathbf{H}_{i,:}$ is the i -th row of \mathbf{H} . This can be performed in parallel for each index i . Since in this case i are integers and `Rimu.jl` operators are indexed by Fock addresses, a translation layer is used to convert between them, and the off-diagonal elements of \mathbf{H} are generated on the fly as described in Sec. 6.2. While these matrix-free methods are much slower than the methods employing sparse matrices, we only need to store the vectors and the translation layer in memory, which allows us to solve much larger problems.

6 Data structures

In `Rimu.jl` we refer to Fock addresses that are compact representations of many-body states and form the basis for the coefficient vectors \mathbf{c} . Because the basis is so large for typical many-body problems we need to store the coefficient vectors as sparse vectors that can be indexed by Fock addresses. Operators that act on the vectors, including Hamiltonians, are also indexed by Fock addresses but without storing the matrix elements in memory. Efficient realisation of vector–vector and matrix–vector products depends on the implementation of these key data structures. In this section we discuss Fock space addresses in Sec. 6.1, Hamiltonians and other operators in Sec. 6.2 and vectors in Sec. 6.3. Finally, in 6.4 we discuss how a matrix–vector product is parallelised and distributed.

For a more thorough treatment of the types and interfaces, as well as usage examples, please consult the project documentation¹.

6.1 Fock state addresses

`Rimu.jl` is primarily designed to work with quantum many-body Hamiltonians. To represent them as matrices, we use a Fock basis

$$|n_1, n_2, \dots, n_M\rangle = \prod_{i=1}^M \frac{1}{\sqrt{n_i!}} \left(\hat{a}_i^\dagger\right)^{n_i} |\text{vac}\rangle, \quad (29)$$

where \hat{a}_i^\dagger is the creation operator for either a boson or a fermion, $N = \sum_{i=1}^M n_i$ is the number of particles, M is the number of modes (sites) indexed by i , and $|\text{vac}\rangle$ is the vacuum state with no particles. In `Rimu.jl`, a Fock state may be a `SingleComponentFockAddress`, or a `CompositeFS`. The former is used to represent a single component of bosons or fermions and includes the following concrete types

- `BoseFS{N, M}`: Bosonic Fock states with a fixed number of particles N in M modes.
- `FermiFS{N, M}`: Fermionic Fock states with a fixed number of particles N in M modes.

¹<https://RimuQMC.github.io/Rimu.jl/stable/>

- `OccupationNumberFS{M}`: Bosonic Fock state with M modes. The particle number is not part of the type specification but run-time data for this type. This type is useful for Hamiltonians that do not conserve particle number.

The remaining type, `CompositeFS{M}` is used to represent an arbitrary mixture of single-component addresses with M modes.

Since we want to work with very large vectors, it is extremely important to have compact representations of bosonic and fermionic Fock states available. To achieve this, `BoseFS` and `FermiFS` are represented either by bitstrings, or sorted particle lists. Which representation is used is determined automatically at compile time, depending on which one is more compact. The bitstrings are packed into unsigned integers of appropriate size, *e.g.* a 9-bit bitstring would be stored in a 16-bit integer. If the number of bits is larger than 64, an appropriate number of 64-bit integers is used. The sorted particle list is a sorted sequence of integers, where each integer represents a particle, and its value represents the mode the particle is in. The width of the integers is determined automatically to allow for the specified number of modes M and the list is kept sorted to ensure a one-to-one correspondence between the data structure and Fock states, which represent indistinguishable particles. Sorted particle lists are used only when $M \gg N$.

Fock states are constructed by either passing the occupation number representation to the appropriate constructor:

```
julia> BoseFS(0, 3, 0)
BoseFS{3,3}(0, 3, 0)
```

or by specifying the number of modes followed by (position, occupation number)-pairs:

```
julia> BoseFS(3, 2 => 3)
BoseFS{3,3}(0, 3, 0)
```

In some cases, Fock states are printed in a compact string representation. This output can be copied back to the Julia REPL and used as a constructor:

```
julia> print(IOContext(stdout, :compact=>true), BoseFS(0, 3, 0))
fs"|0 3 0"

julia> fs"|0 3 0"
BoseFS{3,3}(0, 3, 0)
```

In the bitstring `BoseFS` representation, a sequence of ones is used to represent the number of bosons in a mode, and zeros are used as separators between modes. This representation requires $N + M - 1$ bits.

```
julia> bitstring(BoseFS(1, 0, 1))
"1001"
julia> bitstring(BoseFS(0, 2, 3, 4, 0, 1))
"100111101110110"
```

Note that the bitstring is stored in reversed order.

Fermionic addresses behave in largely the same way as the bosonic ones, but do not allow for more than one particle in the same mode.

```

julia> FermiFS(1, 0, 1)
FermiFS{2,3}(1, 0, 1)
julia> FermiFS(3, 1 => 1, 3 => 1)
FermiFS{2,3}(1, 0, 1)

julia> FermiFS(2, 0, 1)
ERROR: ArgumentError: Invalid ONR: may only contain 0s and 1s.

```

A FermiFS bitstring is simple — each bit in the bitstring represents a mode and its value indicates whether the mode is occupied or not. This requires M bits to store the state regardless of particle number.

```

julia> bitstring(FermiFS(1, 0, 1))
"101"
julia> bitstring(FermiFS(1, 0, 1, 0, 0, 1, 1))
"1100101"

```

The non-particle number-conserving OccupationNumberFS uses a different representation. This type of address is represented by a sequence of M integers, each representing the occupation number in a given mode. The width of these integers determines the maximum number of particles allowed per mode. It defaults to `UInt8`, which allows for a maximum of 255 particles per mode.

```

julia> OccupationNumberFS(1, 2, 34)
OccupationNumberFS{3, UInt8}(1, 2, 34)

julia> OccupationNumberFS{4, UInt16}(1, 2, 256, 511)
OccupationNumberFS{4, UInt16}(1, 2, 256, 511)

```

For mixtures, CompositeFS is available. It is a container that holds any number of other addresses with the same mode number M . It can be constructed by passing other non-composite addresses.

```

julia> composite_address = CompositeFS(
    BoseFS(1, 0, 1),
    FermiFS(1, 0, 1),
    FermiFS(0, 1, 0),
)
CompositeFS(
    BoseFS{2,3}(1, 0, 1),
    FermiFS{2,3}(1, 0, 1),
    FermiFS{1,3}(0, 1, 0),
)

```

To make writing operators that act on the Fock states more convenient, the `excitation` function is provided. As an example, suppose that we want to apply

$$\hat{a}_3^\dagger \hat{a}_5 \quad (30)$$

to the fermionic Fock state $|1001101\rangle$, ie. a particle in mode 5 is moved to mode 3. In code, this is done as follows. First, we define the state

```
julia> state = FermiFS(1, 0, 0, 1, 1, 0, 1);
```

Next, we use the `find_mode` function to get pointers to the 3rd and 5th sites in the address.

```
julia> i, j = find_mode(state, (3, 5));
```

Finally, we apply the `excitation` function, which takes as its arguments the state and the modes where particles are to be created and annihilated. The new state and the value associated with applying the operator are returned:

```
julia> excitation(state, (i,), (j,))  
(FermiFS{4,7}(1, 0, 1, 1, 0, 0, 1), -1.0)
```

Using multiple dispatch, these tools can be used to write functions that will work on both fermionic and bosonic addresses and will take fermionic antisymmetry into account. Note that the same function can be used for excitations that involve any number of particles.

6.2 Hamiltonians and operators

Hamiltonians, conceptually, can be represented as matrices (of, possibly, enormous size) with elements that are the overlap integrals of the Hamiltonian operator between the states of the Fock basis. For problems where the state is represented by a very large vector, which may itself only represent a subset of an even larger Hilbert space, it is impractical to represent operators in the standard way using dense (or sparse) matrices. To use an operator \hat{A} with matrix-free linear algebra routines [39, 48, 50] and FCIQMC, only two operations are required, performing the operator-vector product $\hat{A}|\Psi\rangle$ and stochastically selecting an element from a matrix column with known probability.

In `Rimu.jl`, this is implemented with the `operator_column(A, j)` function, which, conceptually, represents

$$\hat{A}|j\rangle = \sum_i |i\rangle \langle i|\hat{A}|j\rangle, \quad (31)$$

where j is the column address and i represents all reachable addresses with non-zero matrix element $\langle i|\hat{A}|j\rangle$. When computing the elements in a column for an operator that can be written in second quantized form, reachable addresses i and matrix elements $\langle i|\hat{A}|j\rangle$ can be efficiently computed on the fly from j . Then, the product of \hat{A} with a state $|\Psi\rangle$ can be written as

$$\hat{A}|\Psi\rangle = \sum_j \hat{A}|j\rangle \langle j|\Psi\rangle. \quad (32)$$

This can be evaluated without storing the matrix elements $\langle i|\hat{A}|j\rangle$ in memory, which can reduce the memory requirements of exact diagonalisation routines by orders of magnitude, allowing us to study systems much larger than would otherwise have been possible. Stochastic sampling is similar — the sampled matrix element $\langle i|\hat{A}|j\rangle$ and address i can be generated directly from the address j .

When an operator is only intended to be used as an observable, generating the column is not required. Instead, we allow for the direct definition of the overlap

$$\langle \Phi|\hat{A}|\Psi\rangle \quad (33)$$

in terms of the Julia `dot` function. To facilitate the two use-cases of operators in `Rimu.jl`, we define the following type hierarchy:

```
AbstractHamiltonian <: AbstractOperator <: AbstractObservable
```

The `AbstractObservable` is the most permissive type and only supports three-argument dot products `dot(::AbstractDVec, ::AbstractObservable, ::AbstractDVec)`. The next type, `AbstractOperator`, allows the generation of diagonal and off-diagonal elements from a given Fock state. Dot products, vector-operator products and conversion to Julia (sparse) matrices are implemented for `AbstractOperator`. The last type, `AbstractHamiltonian`, is used for model Hamiltonians and implements the interface of `AbstractOperator`, as well as `starting_address`, which returns a Fock state address. This address is used to start an FCIQMC computation and defines the address type and the Hilbert (sub)space in which the operator is represented. While we have defined the operators in terms of Fock states, Rimu.jl is agnostic to what the basis of its operators is. Addresses can in principle be of any type.

As an example, consider the 1D Bose-Hubbard model with strong interactions and 12 particles in 12 sites as seen in the example (see Sec. 2).

```
julia> hamiltonian = HubbardRealSpace(near_uniform(BoseFS{12,12})); u=6)
```

While the `hamiltonian` represents a matrix of size $1,352,078^2$, only 24 bytes are required to store it in memory:

```
julia> dimension(hamiltonian)  
1352078  
julia> sizeof(hamiltonian)  
24
```

The only things stored in the Hamiltonian object are the starting address, its parameters, and information about its geometry.

The matrix elements of the Hamiltonian can be accessed through the `operator_column` function, which returns an object representing a matrix column indexed by a given address

```
julia> column = operator_column(hamiltonian, near_uniform(BoseFS{12,12}))
```

The column can then be used to extract the diagonal element

```
julia> diagonal_element(column)  
0.0
```

and a lazy iterator over the off-diagonal elements.

```
julia> ods = offdiagonals(column)
24-element Rimu.Hamiltonians.HubbardRealSpaceColumnOffdiagonals{Float64, BoseFS{12, 12, BitString{23, 1, UInt32}}, CubicGrid{1, (12,), (true,)}, Tuple{Rimu.Hamiltonians.HubbardRealSpaceComponentData{Float64, 1, 1, CubicGrid{1, (12,), (true,)}, BoseFS{12, 12, BitString{23, 1, UInt32}}}, BoseFS{12, 12, BitString{23, 1, UInt32}}}, Rimu.BitStringAddresses.ModeMap{12, BoseFSIndex}}}}:
fs"|0 2 1 1 1 1 1 1 1 1 1 1" => -1.4142135623730951
fs"|1 0 2 1 1 1 1 1 1 1 1 1" => -1.4142135623730951
fs"|1 1 0 2 1 1 1 1 1 1 1 1" => -1.4142135623730951
fs"|1 1 1 0 2 1 1 1 1 1 1 1" => -1.4142135623730951
...
fs"|1 1 1 1 1 1 1 1 2 0 1 1" => -1.4142135623730951
fs"|1 1 1 1 1 1 1 1 1 2 0 1" => -1.4142135623730951
fs"|1 1 1 1 1 1 1 1 1 1 2 0" => -1.4142135623730951
```

`offdiagonals` here represents all the non-zero elements in the column of the matrix representation of the Hamiltonian except the diagonal element. While the structure returned by `offdiagonals` can be used as a Julia array, it is lazily generated on the fly and as such does not require allocating any memory on the heap. The other way to access off-diagonal elements is through random sampling:

```
julia> random_offdiagonal(column)
(BoseFS{12,12}(1, 1, 1, 1, 1, 1, 1, 1, 0, 2, 1, 1), 0.04166666666666664, -1.4
 142135623730951)
```

This returns the connected address, the probability with which it was selected, and its value. The functions presented here give us enough information about the Hamiltonian to perform exact and sampled matrix-vector products.

6.3 Dict Vectors

Since the Hamiltonians we are interested in operate on vectors that are not indexed by integers, standard (sparse) vectors are not a good fit for Rimu.jl. Instead, we use a dictionary-like structure to represent them. The available implementations of vectors fall under the `AbstractDVec` supertype and generally behave like Julia dictionaries, but will return zero when indexed by an address that is not stored. They can be used in linear algebra operations involving `AbstractHamiltonians`, which were described in more detail in Sec. 6.2. Additionally, they hold a `StochasticStyle`, which tells Rimu.jl how to apply an operator stochastically. Currently, there are three concrete implementations of vectors available: `DVec`, `InitiatorDVec`, and `PDVec`.

The most basic form of `AbstractDVec` is the `DVec`, which is a thin wrapper over a standard Julia dictionary and only supports single-threaded operations. As an example, consider a `DVec`, which is constructed with one or more `address => value` pairs:

```
julia> dvec1 = DVec(BoseFS(1,1,1,1) => 1.0, BoseFS(2,0,2,0) => -1.0)
DVec{BoseFS{4, 4, BitString{7, 1, UInt8}},Float64} with 2 entries, style =
  IsDeterministic{Float64}()
fs"|2 0 2 0" => -1.0
fs"|1 1 1 1" => 1.0
```

As mentioned above, it can be indexed much like a dictionary, but will return zero if the requested key is not stored.

```
julia> dvec1[BoseFS(1, 1, 1, 1)]
1.0

julia> dvec1[BoseFS(4, 0, 0, 0)]
0.0
```

The vector can be multiplied with an operator using the standard multiplication function or its in-place counterpart `LinearAlgebra.mul!`:

```
julia> hamiltonian = HubbardMom1D(BoseFS(1,1,1,1))
HubbardMom1D(fs"|1 1 1 1"; u=1.0, t=1.0)

julia> dvec2 = hamiltonian * dvec1
DVec{BoseFS{4, 4, BitString{7, 1, UInt8}},Float64} with 16 entries, style =
  IsDeterministic{Float64}()
```

```

fs"|"4 0 0 0>" => -0.612372
fs"|"2 2 0 0>" => 1.0
fs"|"3 0 1 0>" => 0.612372
fs"|"1 2 1 0>" => -0.707107
fs"|"2 0 2 0>" => -2.5
fs"|"0 2 2 0>" => 1.0
fs"|"1 0 3 0>" => 0.612372
fs"|"0 0 4 0>" => -0.612372
fs"|"2 1 0 1>" => -0.353553
fs"|"0 3 0 1>" => 0.612372
fs"|"1 1 1 1>" => 3.0
fs"|"0 1 2 1>" => -0.353553
fs"|"2 0 0 2>" => 1.0
fs"|"1 0 1 2>" => -0.707107
fs"|"0 0 2 2>" => 1.0
fs"|"0 1 0 3>" => 0.612372

julia> dvec3 = similar(dvec1)
DVec{BoseFS{4, 4, BitString{7, 1, UInt8}},Float64} with 0 entries, style =
IsDeterministic{Float64}()

julia> mul!(dvec3, hamiltonian, dvec1);

julia> dvec3 == dvec2
true

```

Hamiltonians together with dict vectors (see Sec. 6.2) allow for a wide range of linear algebra operations. The list includes (but is not limited to) vector-operator-vector dot-products, matrix-vector multiplication (and its in-place version with `mul!`).

```

julia> dot (dvec1, dvec2)
3.0

julia> dot (dvec1, hamiltonian, dvec1)
3.0

julia> norm(dvec2)
3.8078865529319543

julia> sum(dvec2)
9.449489742783177

```

6.4 Parallel operations on vectors

The remaining implementation of `AbstractDVec` is `PDVec`, which allows for parallel and distributed operations and is the default choice on multi-core and/or distributed systems.

For most use-cases, a `PDVec` is used in the same manner as a `DVec`, while many operations performed on it are automatically parallelised. Parallelisation is achieved by splitting the storage of the vector into k segments (each being a Julia dictionary) where k is the number of threads available on the system. Then, each (address, value) pair is stored in the segment determined by the hash function of the address. Mathematically, we can think of a `PDVec` \mathbf{p} as being split into subvectors $\mathbf{p}^{(i)}$ with disjoint support

$$\mathbf{p} = \sum_{i=1}^k \mathbf{p}^{(i)}. \quad (34)$$

Then, any element-wise operation on \mathbf{p} including reductions can be performed on each subvector independently. This allows for parallelisation of many functions, such as sums, dot products, vector compression, or any operation defined in terms of `mapreduce`. The

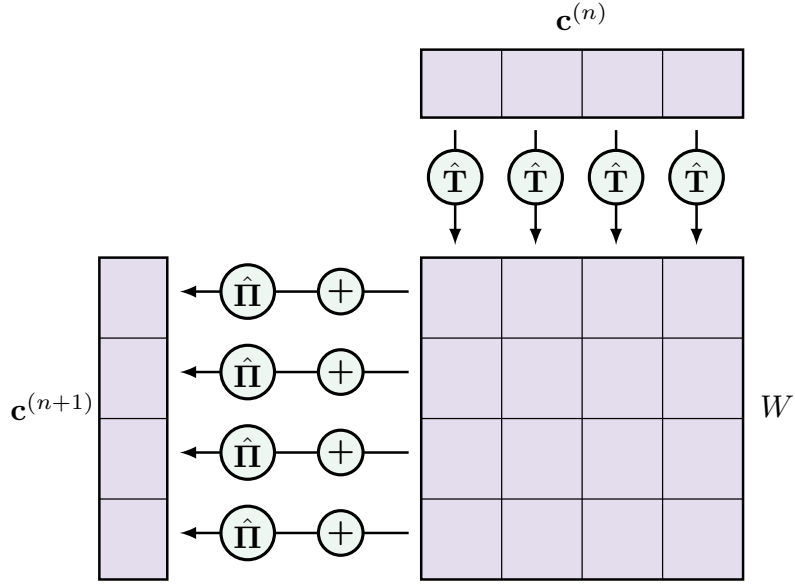


Figure 5: A diagram showing a parallel (multi-threaded) operator-vector product $\check{\mathbf{T}}\mathbf{c}^{(n)}$. Segmentation of the working memory allows for fully parallel processing without race conditions as each core operates on its own memory segment. The operation is performed in two phases. First, the operator $\check{\mathbf{T}}$ is applied to each segment of $\mathbf{c}^{(n)}$ with the result stored column-wise in the working memory W . Then, the segments in W are summed row-wise, (optionally) compressed, and stored to the result vector $\mathbf{c}^{(n+1)}$. The diagram shows a vector split into four segments, which would allow both phases to be performed in parallel on four CPU threads.

matrix-vector multiplication, can also be performed segment-wise as

$$\mathbf{T}\mathbf{p} = \sum_{i=1}^k \mathbf{T}\mathbf{p}^{(i)}. \quad (35)$$

However, since the supports of $\mathbf{T}\mathbf{p}^{(i)}$ are no longer disjoint, performing the sum is not possible until all threads are finished. To avoid this issue, a working memory data structure W is introduced. W is a $k \times k$ array of dictionaries in which each of its rows and columns is organised in the same way as the vector \mathbf{p} . The intermediate result $\mathbf{T}\mathbf{p}^{(i)}$ is stored in the i -th column of the working memory. Finally, to perform the sum in Eq. (35), the rows of W are summed, which can again be done in parallel. A schematic of this process is shown in Figure 5.

Rimu.jl also supports distributed computing using the MPI [35] standard through MPI.jl [52]. In a distributed scenario where there are r MPI ranks with k threads each, the storage of a `PDVec` is divided into rk segments, of which k are stored on each rank. Performing operations on the vector is similar to as described above, except that MPI synchronisation is performed on every reduction or matrix-vector multiplication, and the working memory is now an $rk \times k$ array.

7 Numerical results

7.1 Semistochasticity and vector compression styles

In this section, we discuss how changing the details of the matrix and vector compression algorithms affects the result of an FCIQMC calculation. Specifically, we look at two ways the algorithm described in Sec. 3.2 can be modified in `Rimu.jl`.

To provide a quantitative comparison, we will look at a measure of statistical efficiency, which is based on one introduced in Ref. [27]. We define it as

$$f = (\sigma_{\bar{S}}^2 \Omega \tilde{t})^{-1} \quad (36)$$

where $\sigma_{\bar{S}}$ is the (blocked) error estimate of the mean of the shift, Ω is the number of time steps (not including the equilibration phase), and \tilde{t} is the median of the wall time taken to perform one FCIQMC step. Note that this definition differs from the one defined in Ref. [27] in the inclusion of the median of the wall-time in the measure. We include it because changing the compression algorithm often results in better statistics at a cost of more CPU time required per step. All measurements in this section were performed as single-threaded computations.

Late and early compression — In Sec. 3.2, we apply the stochastic vector projection operator $\check{\Pi}$ after the stochastic operator \check{T} has been sampled and the contributions from the different parts of the input vector \mathbf{c} have been summed, *i.e.*,

$$\check{T}\mathbf{c} = \check{\Pi} \left(\sum_i \tilde{T}_{:,i} c_i \right). \quad (37)$$

We will refer to this approach as late compression. An alternative (standard [9, 31]) approach, which we call early compression, is to apply the compression operator to each spawn individually as

$$\check{T}'\mathbf{c} = \sum_i \check{\Pi} \tilde{T}_{:,i} c_i. \quad (38)$$

These approaches are equivalent on average. The only difference between them is whether annihilation is done before or after compression. Because of this, early compression is more efficient to compute, while late compression produces better statistics.

The results of comparisons between the two vector compression algorithms are shown in Figs. 6 and 7. We note that in all cases, applying compression late has the effect of reducing error bar size, while increasing the runtime per step. These competing effects appear to provide an overall benefit when the FCIQMC instantaneous vector is peaked significantly. This can be explained by the fact that there, configurations in the vector with small coefficient values are allowed to spawn to larger ones uncompressed. On top of that, several small spawns hitting the same configuration are compressed less severely than they would have been otherwise.

When the system has a sign problem (Fig. 6), the difference between the two methods is dramatic. There, we notice that by applying late compression, the sign problem is overcome at a smaller value of N_t and the statistical efficiency is increased considerably. Reducing the relative semistochastic threshold t_{rel} increases statistical efficiency further, but does not appear to affect the sign problem at all. Panels (c) and (d) show a similar result with projected energy \bar{E}_y with a simple single-configuration projector. There, we see the error bars drop drastically once the sign problem is overcome, while the statistical efficiency follows a pattern similar to what is shown in panel b). In such cases, applying compression late is strictly better than applying it early.

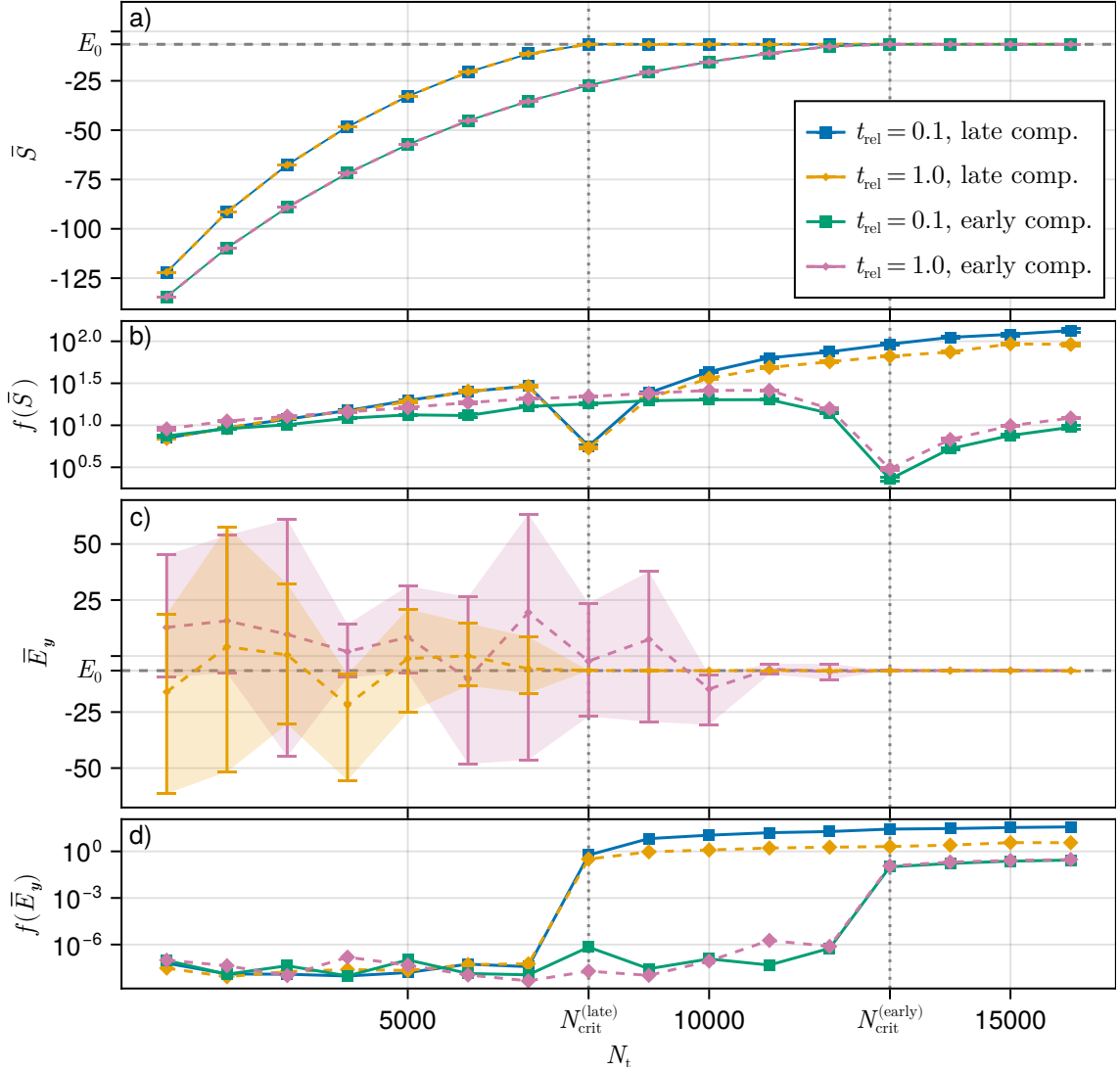


Figure 6: The effect of late compression on the sign problem. The plot shows (a) the mean of the shift $\langle \bar{S} \rangle$ and (b) the statistical efficiency of the shift $f(\langle \bar{S} \rangle)$. The FCIQMC computations were performed with a momentum space Bose Hubbard model with $N = 10$ particles in $M = 10$ momentum modes with strong interactions at $u = 6$ and a hopping strength of $t = 1$. Each point in the plots is an average obtained from a time series of 10^7 steps at $\delta\tau = 10^{-3}$, where the first 10^5 steps were discarded.

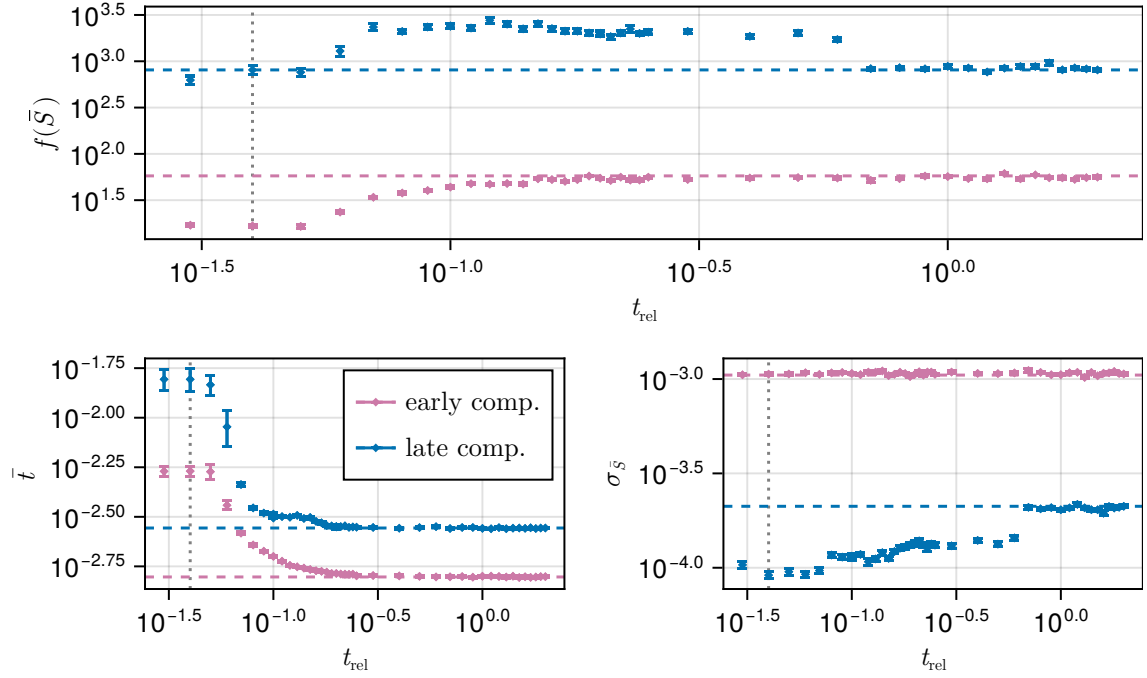


Figure 7: The effect of the relative semistochastic threshold t_{rel} and late compression on the statistical efficiency of the shift $f(\langle S \rangle)$, the median time per step \bar{t} , and the (blocked) error bar size $\sigma_{\bar{S}}$. The FCIQMC computations were performed with a real space Bose Hubbard model with $N = 12$ particles in $M = 12$ modes with strong interactions at $u = 6$ and a hopping strength of $t = 1$. The horizontal dashed lines represent a setting of $t_{\text{rel}} = \infty$, *i.e.*, no semistochasticity. The gray vertical dotted line represents a threshold where all of the spawns in the FCIQMC run are performed exactly.

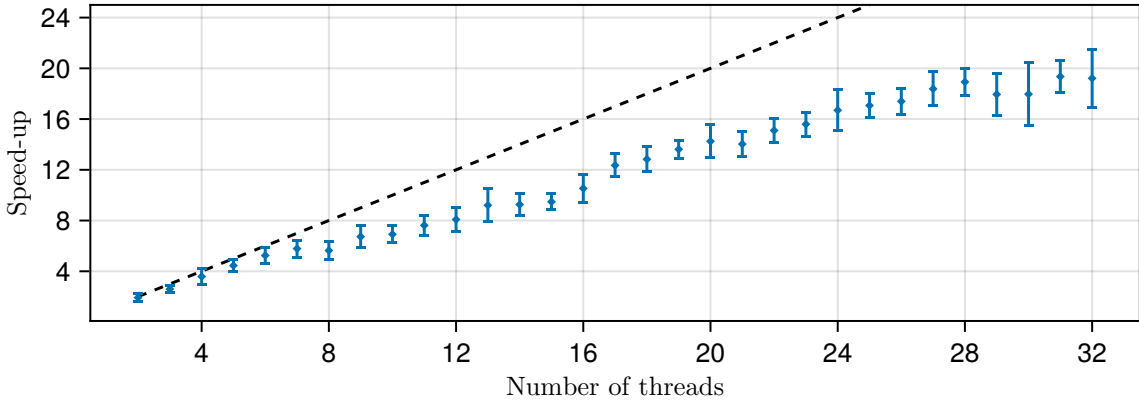


Figure 8: Scaling of shared memory parallelism. The speed-up relative to one thread for a multithreaded FCIQMC computation. The dashed black line shows the ideal linear scaling. In this regime, the speed-up is roughly linear with a slope of 0.61.

Semistochastic threshold — In Eq. (16), we note that we perform an exact spawning step if the coefficient value c_i is larger than the number of non-zero off-diagonal elements in a column of the matrix \mathbf{T} . This can be modified by introducing a semistochastic threshold t_{rel} and performing the exact step if $c_i t_{\text{rel}} \geq m_i$. Setting a lower value t_{rel} forces the algorithm to take more exact steps, which reduces the noise in the algorithm, while setting a higher value is more time-efficient. These competing effects cancel favourably, and a larger statistical efficiency is achieved, as shown in Fig. 7. However, this is highly Hamiltonian dependent and the effects are not always as dramatic as those presented in Fig. 7. The default value of $t_{\text{rel}} = 1$ often works well enough in practical situations.

7.2 Performance benchmarks

In this section, we present performance benchmarks that demonstrate how FCIQMC computations scale when a large number of threads or computer nodes is utilised. All presented benchmarks were performed with the two-dimensional Bose–Hubbard model with $N = 36$ particles in $M = 6 \times 6$ sites, an interaction strength of $u = 1$ and a hopping strength of $t = 0.1$ modified with a Gutzwiller importance sampling ansatz [22]. This is a system in the superfluid regime, where the ground state wavefunction is spread out across the Hilbert space, making it a somewhat difficult problem for FCIQMC to solve. The dimension of the Hamiltonian in question is 7.97×10^{21} .

Single-node multithreading — Figure 8 shows the result of the first benchmark, where we measure the multithreading scaling on a single computer node. The number of walkers was set to $N_t = 10^7$. In each benchmark, we perform a 25,000-step equilibration, after which we measure the wall-time it takes to perform 50,000 steps. Then, each such benchmark is repeated 8 times, and the average and standard deviation between the 8 runs is reported. As seen in Fig. 8, the scaling is favourable – 32 threads presents a 20-fold speed-up compared to a single-threaded computation, performing over 112 steps per second on average.

Multi-node parallelism — For measuring how Rimu.jl performs in a multi-node distributed setting, we employed the resources of the Frontier supercomputer at the Oak Ridge National Laboratory. There, each compute node consists of a 64-core AMD Optimized 3rd Gen EPYC CPU, with 56 allocatable cores under the so-called low-noise mode layout, *i.e.*, 8 CPUs are reserved system processes. We have performed the benchmarks on

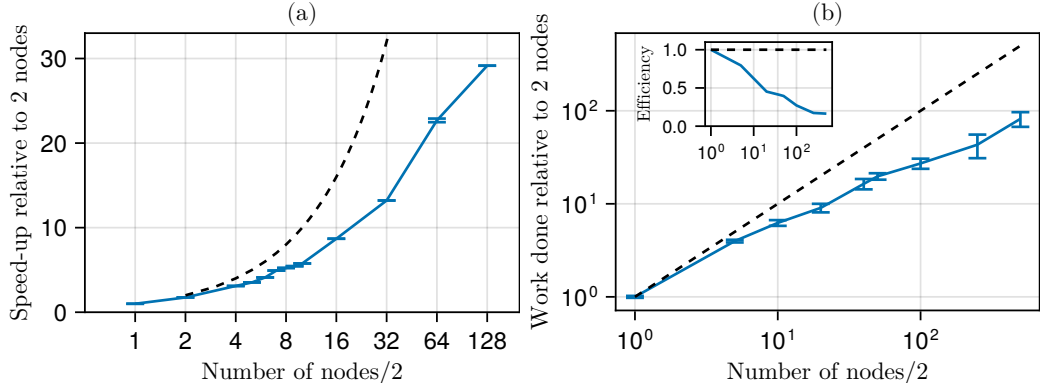


Figure 9: Scaling of multi-node parallelism. (a) The speed-up relative to 2 nodes of the average wall-time for performing a single FCIQMC step with Rimu.jl with 10^9 walkers using up to 256 nodes with 14,336 processors. The dashed line shows the ideal linear scaling. (b) The weak-scaling tests from the average wall-time for performing a single FCIQMC step. The main plot shows the relative work done, which is the number of walkers processed per time unit compared to the computation running on two nodes. The dashed line shows the ideal scaling. The inset shows the scaling efficiency calculated as $(\text{walkers processed on } N \text{ nodes}) / (N/2 \times \text{walkers processed on 2 nodes})$ in a fixed amount of time.

the same 6×6 Bose-Hubbard model described above, but have used much larger numbers of walkers, up to 5.6×10^9 in total.

Strong scaling — For the first test, we look at strong scaling. It measures how using more computing power affects the time it takes to get a solution. Ideally, increasing the computational resources by a factor of N would yield an N -fold speed-up. We present the results of benchmarks performed with 10^9 walkers in Fig. 9(a). While the obtained speed-up trails the ideal scaling, Rimu.jl’s performance maintains a general upward trajectory with no visible plateau.

Weak scaling — In the second test, we look at weak scaling. Here, both the size of the problem and the computational resources increase at the same rate. An algorithm that scales ideally would take the same amount of time for all samples taken this way. In this case, we have set Rimu.jl to use 5,600,000 walkers per node and we have run the benchmarks on up to 1000 nodes. In Fig. 9(b), we present the scaling results. We again see less than ideal scaling, however the amount of work done is increasing steadily even up to 1000 nodes. There, we see a six-fold slow-down, which corresponds to the efficiency dropping to around 0.16 for the largest calculations.

The observed reductions in efficiency for these very large calculations could be due to a number of different issues. Time spent on communication and copying data between the nodes is a potential contributing issue that will get worse when the number of nodes is increased. However, we assume that the most important issue is the unequal distribution of workload between the parallel nodes and processes. In order to perform walker annihilations in the FCIQMC algorithm, all nodes are synchronised in each time step, i.e. all nodes must wait for the slowest. In the current implementation, the distribution of configuration-coefficient pairs to the nodes (determining the workload) for processing is done passively through a hashing process, i.e. by (pseudo) random assignment.

The scaling benchmarks of this section show that significant performance gains could be obtained by optimising the code for large-scale computations. We expect that the largest improvement could be gained by an implementation of active load-balancing, which

has improved the efficiency for large-scale computations with similar codebases [31, 32]. However, for many research-grade projects, such large calculations are not necessary and single or few-node calculations suffice. The Rimu.jl codebase runs efficiently with such smaller computations running on a single or a small number of nodes. The results published in Refs. [14–17, 41] were all generated using Rimu.jl with such smaller computations.

8 Conclusion and outlook

We have presented Rimu.jl, a Julia package that implements quantum mechanical Hamiltonians and allows us to diagonalise them exactly or with the full configuration interaction quantum Monte Carlo (FCIQMC) algorithm. By utilising Julia’s rich type system to encode the Fock states, Hamiltonians, and vectors, we are able to solve problems much larger than would have been possible with standard linear algebra algorithms. In addition, the code can be used on parallel and distributed systems. We have discussed the FCIQMC algorithm, key implementation details of the package, and presented benchmarks performed on a large-scale distributed system.

Rimu.jl currently supports Hamiltonians for lattice problems in real and momentum space with on-site and extended interactions, continuum momentum space and transcorrelated [40] Hamiltonians, harmonic oscillator basis and the Frölich polaron Hamiltonians. A `MolecularHamiltonian` type for performing quantum chemistry calculations and a link to the quantum chemistry package `ElemCo.jl` [53] were recently added through a Google Summer of Code project [54]. Some implemented observables include density-density correlations, reduced density matrices and momentum density. Future work could include new Hamiltonians such as spin-orbit coupling systems or hardcore boson Hamiltonians. While these would require the definitions of new Fock state types, such additions are easy to make either as part of or outside of Rimu.jl due to the design of the package combined with Julia’s multiple-dispatch and just-in-time compilation capabilities. Some features of Rimu.jl include excited state calculation [28], the initiator approximation [19], importance sampling [21, 22], and thread-parallel and MPI-distributed [35] calculations. Future work may include extending the algorithm with modern features like the adaptive shift method [20], preconditioning [23, 24], or improved load balancing. A Rimu.jl extension for importance sampling and variational Monte Carlo is available through the (currently unregistered) `Gutzwiller.jl`² package.

The package is under active development with new Hamiltonians, observables, and features being added regularly. Please consult the project documentation³ for an up-to-date list of available Hamiltonians and features. The project is open-source and is licenced under the MIT licence. Contributions from the community in the form of issues or pull requests with code for bug fixes or new features are welcome.

Acknowledgements

The authors would like to thank Jamie Taylor, Satyanand Kuwar, Chuhao Li, Rohan Kumar, Alex Pletzer, Emma Wang, Tilak Patel, and Chris Scott for their contributions to the code and Ali Alavi and Daniel Kats for inspiration and helpful discussions.

²<https://github.com/RimuQMC/Gutzwiller.jl>

³<https://RimuQMC.github.io/Rimu.jl/stable/>

Funding information M.Č., C.J.B., and J.B. received funding from the Marsden Fund of New Zealand (Contract No. MAU 2007), from government funding managed by the Royal Society of New Zealand Te Apārangi. We acknowledge support by the New Zealand eScience Infrastructure (NeSI/REANNZ) high-performance computing facilities in the form of a merit project allocation and a software consultancy project. This research used resources of the Oak Ridge Leadership Computing Facility at the Oak Ridge National Laboratory, which is supported by the Office of Science of the U.S. Department of Energy under Contract No. DE-AC05-00OR22725.

References

- [1] M. P. Nightingale and C. J. Umrigar, *Quantum Monte Carlo Methods in Physics and Chemistry*, Springer Science & Business Media, ISBN 978-0-7923-5552-6 (1998).
- [2] F. Becca and S. Sorella, *Contents*, In *Quantum Monte Carlo Approaches for Correlated Systems*, pp. v–viii. Cambridge University Press, Cambridge, ISBN 978-1-107-12993-1 (2017).
- [3] C. J. Umrigar, *Observations on variational and projector Monte Carlo methods*, The Journal of Chemical Physics **143**(16), 164105 (2015), doi:[10.1063/1.4933112](https://doi.org/10.1063/1.4933112).
- [4] M. H. Kalos, *Monte Carlo Calculations of the Ground State of Three- and Four-Body Nuclei*, Physical Review **128**(4), 1791 (1962), doi:[10.1103/PhysRev.128.1791](https://doi.org/10.1103/PhysRev.128.1791).
- [5] M. H. Kalos, *Stochastic wave function for atomic helium*, Journal of Computational Physics **1**(2), 257 (1966), doi:[10.1016/0021-9991\(66\)90006-4](https://doi.org/10.1016/0021-9991(66)90006-4).
- [6] P. J. Reynolds, J. Tobochnik and H. Gould, *Diffusion Quantum Monte Carlo*, Computer in Physics **4**(6), 662 (1990), doi:[10.1063/1.4822960](https://doi.org/10.1063/1.4822960).
- [7] S. Zhang and H. Krakauer, *Quantum Monte Carlo Method using Phase-Free Random Walks with Slater Determinants*, Physical Review Letters **90**(13), 136401 (2003), doi:[10.1103/PhysRevLett.90.136401](https://doi.org/10.1103/PhysRevLett.90.136401).
- [8] A. Sarsa, K. E. Schmidt and W. R. Magro, *A path integral ground state method*, The Journal of Chemical Physics **113**(4), 1366 (2000), doi:[10.1063/1.481926](https://doi.org/10.1063/1.481926).
- [9] G. H. Booth, A. J. W. Thom and A. Alavi, *Fermion Monte Carlo without fixed nodes: A game of life, death, and annihilation in Slater determinant space*, J. Chem. Phys. **131**(5), 054106 (2009), doi:[10.1063/1.3193710](https://doi.org/10.1063/1.3193710).
- [10] D. M. Cleland, G. H. Booth and A. Alavi, *A study of electron affinities using the initiator approach to full configuration interaction quantum Monte Carlo*, The Journal of Chemical Physics **134**(2), 024112 (2011), doi:[10.1063/1.3525712](https://doi.org/10.1063/1.3525712).
- [11] C. Daday, S. Smart, G. H. Booth, A. Alavi and C. Filippi, *Full Configuration Interaction Excitations of Ethene and Butadiene: Resolution of an Ancient Question*, Journal of Chemical Theory and Computation **8**(11), 4441 (2012), doi:[10.1021/ct300486d](https://doi.org/10.1021/ct300486d).
- [12] J. J. Shepherd, G. Booth, A. Grüneis and A. Alavi, *Full configuration interaction perspective on the homogeneous electron gas*, Physical Review B **85**(8), 081103 (2012), doi:[10.1103/PhysRevB.85.081103](https://doi.org/10.1103/PhysRevB.85.081103).

[13] O. Weser, L. Freitag, K. Guther, A. Alavi and G. Li Manni, *Chemical insights into the electronic structure of Fe(II) porphyrin using FCIQMC, DMRG, and generalized active spaces*, International Journal of Quantum Chemistry **121**(3), e26454 (2021), doi:[10.1002/qua.26454](https://doi.org/10.1002/qua.26454).

[14] J. Taylor, M. Čufar, D. Mitrouskas, R. Seiringer, E. Pahl and J. Brand, *Bound excited states of Fröhlich polarons in one dimension*, Physical Review B **112**(18), 184312 (2025), doi:[10.1103/s9p9-jflq](https://doi.org/10.1103/s9p9-jflq).

[15] R. Alhyder, V. Colussi, M. Čufar, J. Brand, A. Recati and G. M. Bruun, *Lattice Bose polarons at strong coupling and quantum criticality*, SciPost Physics **19**(1), 002 (2025), doi:[10.21468/SciPostPhys.19.1.002](https://doi.org/10.21468/SciPostPhys.19.1.002).

[16] L. Rammelmüller, D. Huber, M. Čufar, J. Brand, H.-W. Hammer and A. G. Volosniev, *Magnetic impurity in a one-dimensional few-fermion system*, SciPost Physics **14**(1), 006 (2023), doi:[10.21468/SciPostPhys.14.1.006](https://doi.org/10.21468/SciPostPhys.14.1.006).

[17] M. Yang, M. Čufar, E. Pahl and J. Brand, *Polaron-Depletion Transition in the Yrast Excitations of a One-Dimensional Bose Gas with a Mobile Impurity*, Condensed Matter **7**(1), 15 (2022), doi:[10.3390/condmat7010015](https://doi.org/10.3390/condmat7010015).

[18] F. R. Petruzielo, A. A. Holmes, H. J. Changlani, M. P. Nightingale and C. J. Umrigar, *Semistochastic Projector Monte Carlo Method*, Physical Review Letters **109**(23), 230201 (2012), doi:[10.1103/PhysRevLett.109.230201](https://doi.org/10.1103/PhysRevLett.109.230201).

[19] D. Cleland, G. H. Booth and A. Alavi, *Communications: Survival of the fittest: Accelerating convergence in full configuration-interaction quantum Monte Carlo*, J. Chem. Phys. **132**(4), 041103 (2010), doi:[10.1063/1.3302277](https://doi.org/10.1063/1.3302277).

[20] K. Ghanem, K. Guther and A. Alavi, *The adaptive shift method in full configuration interaction quantum Monte Carlo: Development and applications*, The Journal of Chemical Physics **153**(22), 224115 (2020), doi:[10.1063/5.0032617](https://doi.org/10.1063/5.0032617).

[21] C. J. Umrigar, M. P. Nightingale and K. J. Runge, *A diffusion Monte Carlo algorithm with very small time-step errors*, The Journal of Chemical Physics **99**(4), 2865 (1993), doi:[10.1063/1.465195](https://doi.org/10.1063/1.465195).

[22] K. Ghanem, N. Liebermann and A. Alavi, *Population control bias and importance sampling in full configuration interaction quantum Monte Carlo*, Phys. Rev. B **103**(15), 155135 (2021), doi:[10.1103/PhysRevB.103.155135](https://doi.org/10.1103/PhysRevB.103.155135).

[23] N. S. Blunt, A. J. W. Thom and C. J. C. Scott, *Preconditioning and Perturbative Estimators in Full Configuration Interaction Quantum Monte Carlo*, Journal of Chemical Theory and Computation **15**(6), 3537 (2019), doi:[10.1021/acs.jctc.9b00049](https://doi.org/10.1021/acs.jctc.9b00049).

[24] V. A. Neufeld and A. J. W. Thom, *Accelerating Convergence in Fock Space Quantum Monte Carlo Methods*, Journal of Chemical Theory and Computation **16**(3), 1503 (2020), doi:[10.1021/acs.jctc.9b01023](https://doi.org/10.1021/acs.jctc.9b01023).

[25] A. A. Holmes, N. M. Tubman and C. J. Umrigar, *Heat-Bath Configuration Interaction: An Efficient Selected Configuration Interaction Algorithm Inspired by Heat-Bath Sampling*, Journal of Chemical Theory and Computation **12**(8), 3674 (2016), doi:[10.1021/acs.jctc.6b00407](https://doi.org/10.1021/acs.jctc.6b00407).

[26] L.-H. Lim and J. Weare, *Fast Randomized Iteration: Diffusion Monte Carlo through the Lens of Numerical Linear Algebra*, SIAM Rev. **59**(3), 547 (2017), doi:[10.1137/15M1040827](https://doi.org/10.1137/15M1040827).

[27] S. M. Greene, R. J. Webber, J. Weare and T. C. Berkelbach, *Beyond Walkers in Stochastic Quantum Chemistry: Reducing Error Using Fast Randomized Iteration*, Journal of Chemical Theory and Computation **15**(9), 4834 (2019), doi:[10.1021/acs.jctc.9b00422](https://doi.org/10.1021/acs.jctc.9b00422).

[28] N. S. Blunt, S. D. Smart, G. H. Booth and A. Alavi, *An excited-state approach within full configuration interaction quantum Monte Carlo*, The Journal of Chemical Physics **143**(13), 134117 (2015), doi:[10.1063/1.4932595](https://doi.org/10.1063/1.4932595).

[29] N. S. Blunt, T. W. Rogers, J. S. Spencer and W. M. C. Foulkes, *Density-matrix quantum Monte Carlo method*, Physical Review B **89**(24), 245124 (2014), doi:[10.1103/PhysRevB.89.245124](https://doi.org/10.1103/PhysRevB.89.245124).

[30] J. R. McClean and A. Aspuru-Guzik, *Clock quantum Monte Carlo technique: An imaginary-time method for real-time quantum dynamics*, Physical Review A **91**(1), 012311 (2015), doi:[10.1103/PhysRevA.91.012311](https://doi.org/10.1103/PhysRevA.91.012311).

[31] K. Guther, R. J. Anderson, N. S. Blunt, N. A. Bogdanov, D. Cleland, N. Dattani, W. Dobrutz, K. Ghanem, P. Jeszenszki, N. Liebermann, G. L. Manni, A. Y. Lozovoi *et al.*, *NECI: N-Electron Configuration Interaction with an emphasis on state-of-the-art stochastic methods*, The Journal of Chemical Physics **153**(3), 034107 (2020), doi:[10.1063/5.0005754](https://doi.org/10.1063/5.0005754).

[32] J. S. Spencer, N. S. Blunt, S. Choi, J. Etrych, M.-A. Filip, W. M. C. Foulkes, R. S. T. Franklin, W. J. Handley, F. D. Malone, V. A. Neufeld, R. Di Remigio, T. W. Rogers *et al.*, *The HANDE-QMC Project: Open-Source Stochastic Quantum Chemistry from the Ground State Up*, Journal of Chemical Theory and Computation **15**(3), 1728 (2019), doi:[10.1021/acs.jctc.8b01217](https://doi.org/10.1021/acs.jctc.8b01217).

[33] S. M. Greene and C. Frech, *FRIES* (2019).

[34] J. Bezanson, A. Edelman, S. Karpinski and V. B. Shah, *Julia: A fresh approach to numerical computing*, SIAM Review **59**(1), 65 (2017), doi:[10.1137/141000671](https://doi.org/10.1137/141000671).

[35] Message Passing Interface Forum, *MPI: A Message-Passing Interface Standard Version 4.1* (2023).

[36] M. P. A. Fisher, P. B. Weichman, G. Grinstein and D. S. Fisher, *Boson localization and the superfluid-insulator transition*, Phys. Rev. B **40**, 546 (1989), doi:[10.1103/PhysRevB.40.546](https://doi.org/10.1103/PhysRevB.40.546).

[37] *SciML/CommonSolve.jl*, SciML Open Source Scientific Machine Learning (2025).

[38] M. Bouchet-Valat and B. Kamiński, *DataFrames.jl: Flexible and Fast Tabular Data in Julia*, Journal of Statistical Software **107**, 1 (2023), doi:[10.18637/jss.v107.i04](https://doi.org/10.18637/jss.v107.i04).

[39] J. Haegeman, *KrylovKit*, Zenodo, doi:[10.5281/zenodo.14911568](https://doi.org/10.5281/zenodo.14911568) (2025).

[40] P. Jeszenszki, U. Ebling, H. Luo, A. Alavi and J. Brand, *Eliminating the wave-function singularity for ultracold atoms by a similarity transformation*, Physical Review Research **2**(4), 043270 (2020), doi:[10.1103/PhysRevResearch.2.043270](https://doi.org/10.1103/PhysRevResearch.2.043270).

[41] T. G. Backert, F. Brauneis, M. Čufar, J. Brand, H.-W. Hammer and A. G. Volosniev, *Effective Theory for Strongly Attractive One-Dimensional Fermions*, Physical Review Letters **135**(4), 040401 (2025), doi:[10.1103/8mnc-x42q](https://doi.org/10.1103/8mnc-x42q).

[42] M. Yang, E. Pahl and J. Brand, *Improved walker population control for full configuration interaction quantum Monte Carlo*, The Journal of Chemical Physics **153**(17), 174103 (2020), doi:[10.1063/5.0023088](https://doi.org/10.1063/5.0023088).

[43] J. S. Spencer, N. S. Blunt and W. M. Foulkes, *The sign problem and population dynamics in the full configuration interaction quantum Monte Carlo method*, J. Chem. Phys. **136**(5), 054110 (2012), doi:[10.1063/1.3681396](https://doi.org/10.1063/1.3681396).

[44] J. Brand, M. Yang and E. Pahl, *Stochastic differential equation approach to understanding the population control bias in full configuration interaction quantum Monte Carlo*, Phys. Rev. B **105**(23), 235144 (2022), doi:[10.1103/PhysRevB.105.235144](https://doi.org/10.1103/PhysRevB.105.235144).

[45] H. Flyvbjerg and H. G. Petersen, *Error estimates on averages of correlated data*, The Journal of Chemical Physics **91**(1), 461 (1989), doi:[10.1063/1.457480](https://doi.org/10.1063/1.457480).

[46] M. Jonsson, *Standard error estimation by an automated blocking method*, Phys. Rev. E **98**(4), 043304 (2018), doi:[10.1103/PhysRevE.98.043304](https://doi.org/10.1103/PhysRevE.98.043304).

[47] F. B. Carlson, *MonteCarloMeasurements.jl: Nonlinear Propagation of Arbitrary Multivariate Distributions by means of Method Overloading*, doi:[10.48550/arXiv.2001.07625](https://arxiv.org/abs/2001.07625) (2020), [2001.07625](https://arxiv.org/abs/2001.07625).

[48] R. B. Lehoucq, D. C. Sorensen and C. Yang, *ARPACK Users' Guide*, Software, Environments, and Tools. Society for Industrial and Applied Mathematics, ISBN 978-0-89871-407-4, doi:[10.1137/1.9780898719628](https://doi.org/10.1137/1.9780898719628) (1998).

[49] *JuliaLinearAlgebra/Arpack.jl*, JuliaLinearAlgebra (2025).

[50] *JuliaLinearAlgebra/IterativeSolvers.jl*, JuliaLinearAlgebra (2025).

[51] *JuliaLinearAlgebra/LinearMaps.jl*, JuliaLinearAlgebra (2025).

[52] S. Byrne, L. C. Wilcox and V. Churavy, *MPI.jl: Julia bindings for the Message Passing Interface*, Proceedings of the JuliaCon Conferences **1**(1), 68 (2021), doi:[10.21105/jcon.00068](https://doi.org/10.21105/jcon.00068).

[53] *fkfest/ElemCo.jl*, MPI-FKF Electronic Structure Theory (2026).

[54] C. Li, E. Pahl, D. Katz and J. Brand, *Ab-Initio Quantum Chemistry with Rimu.jl*, <https://summerofcode.withgoogle.com/archive/2025/projects/rIUIYnPe>.